Scientia Pharmaceutica

ÖSTERREICHISCHE PHARMAZEUTISCHE GESELLSCHAFT

MDPI

Review

A Brief Review of Synthetic Strategies of α-Pyrone-Based Phloroglucinol Derivatives from *Helichrysum* spp. and Structure–Activity Insights

Yulian Voynikov [1], Konstantin Konstantinov [1], Iliyan Ivanov [2] and Stanimir Manolov [2,*]

[1] Department of Chemistry, Faculty of Pharmacy, Medical University, 1000 Sofia, Bulgaria; y_voynikov@pharmfac.mu-sofia.bg (Y.V.); k.konstantinov@pharmfac.mu-sofia.bg (K.K.)

[2] Department of Organic Chemistry, Faculty of Chemistry, University of Plovdiv, 24 "Tsar Assen" Str., 4000 Plovdiv, Bulgaria; iiiliyan@abv.bg

* Correspondence: manolov@uni-plovdiv.bg; Tel.: +359-32-261-348

Abstract

This review summarizes the synthesis and structural modification of α-pyrone-containing phloroglucinol derivatives from *Helichrysum* species. Synthetic routes to both natural products and synthetic analogues are covered, highlighting strategies ranging from β-keto ester cyclodehydration to multicomponent condensations. Key methods include aldehyde-mediated dimerization, fluoride-catalyzed heterodimerization, and acid-catalyzed cyclization to benzopyran frameworks. The reported approaches enabled access to diverse monopyrone, dipyrone, arzanol-type, and cyclized analogues. Additionally, retrosynthetic analyses toward phloroglucinol–pyrone heterodimers are discussed, highlighting convergent synthetic strategies for future access to benzofurane-, chromene-, and chromane-based analogues. This review integrates published experimental data with newly generated in silico predictions.

Keywords: alpha-pyrone; arzanol; *Helichrysum*; phloroglucinol; synthesis; PASS online; in silico pharmacology; toxicity

1. Introduction

Phloroglucinol-based α-pyrones represent synthetically accessible and pharmacologically relevant frameworks. Their modular reactivity has enabled access to structurally diverse derivatives, including monopyrones, dipyrones, and methylene-bridged hybrids. Among them, arzanol and related dipyrone structures have attracted interest due to their potent dual inhibition of microsomal prostaglandin E_2 synthase-1 (mPGES-1) and 5-lipoxygenase (5-LO), two non-redundant targets in eicosanoid biosynthesis [1,2]. The modular nature of α-pyrone synthesis enables diversification via condensation reactions, oxidative transformation, and electrophilic coupling, allowing systematic exploration of side-chain variation and substitution patterns. Previous reports have highlighted the influence of alkylidene linker length and core hydroxylation on both enzyme selectivity and antibacterial potency, particularly against multidrug-resistant *Staphylococcus aureus* [2,3]. In this context, we discuss the preparation of monopyrone and dipyrone derivatives, arzanol analogues, and cyclized scaffolds, alongside their functionalization via acetylation and methylation. Selected compounds were evaluated in vitro for mPGES-1 and 5-LO inhibition, as well as antibacterial activity, to delineate key structure–activity relationships and identify candidates with dual bioactivity.

Academic Editor: William A. Donaldson

Received: 3 June 2026
Revised: 1 July 2026
Accepted: 10 July 2026
Published: 13 July 2026

Here, all reported data on synthetic α-pyrone derivatives from *Helichrysum* available in the literature, to the best of our knowledge, are compiled. The dataset encompasses monopyrones, dipyrones, arzanol-type methylene-bridged hybrids, cyclized analogues, methyl ethers, and acetylated derivatives. For each compound, key chemical, synthetic, and biological details are provided, including structural descriptors, synthetic yields, and biological activity where available. This complete collection offers a structured foundation for guiding future design of *Helichrysum*-derived α-pyrone pharmacophores.

Table A1 presents the synthetic conditions and experimental details for a total of thirty (**1s**–**30s**) α-pyrone-phloroglucinol synthetic derivatives based on *Helichrysum* natural products. The synthetic transformations encompass a diverse range of methodologies, including multicomponent condensations such as helipyrone and arzanol, acid-catalyzed cyclodehydration reactions for monopyrone synthesis, post-synthetic modifications through acetylation and methylation protocols, and intramolecular cyclization reactions generating tricyclic frameworks. The reported yields range from modest conversions in the cyclization reactions of arzanol to cycloarzanol derivatives (6–29%) to quantitative yields achieved in methylation and acetylation transformations. The experimental conditions detailed in Table A1 highlight the versatility of synthetic approaches employed, utilizing various catalytic systems including tetrabutylammonium fluoride for heterodimeric coupling reactions, polyphosphoric acid for pyrone ring formation, and both Lewis and Brønsted acids for intramolecular cyclization processes. This compilation provides synthetic parameters for researchers seeking to access these bioactive scaffolds, offering reproducible protocols that have been successfully applied to both natural product synthesis and the generation of structurally diverse analogues for biological evaluation. Table A2 summarizes the biological activity data for the synthesized α-pyrone-phloroglucinol derivatives, documenting their inhibitory potencies against microsomal prostaglandin E_2 synthase-1 (mPGES-1) and 5-lipoxygenase (5-LO), along with antibacterial activities against multidrug-resistant *Staphylococcus aureus* strains. The structure–activity relationships reveal that arzanol analogues with hexyl substitutions, particularly compounds **14s** and **19s**, exhibited the most potent dual enzyme inhibition with IC_{50} values, while maintaining significant antibacterial efficacy with minimum inhibitory concentrations between 2 and 16 μg/mL against various resistant bacterial strains.

In silico methods, commonly referred to as computational approaches, complement experimental synthesis and bioactivity assays by predicting pharmacological profiles and toxicity of phloroglucinol-α-pyrone derivatives from *Helichrysum* spp. These preliminary powerful tools, such as PASS online, accelerate drug discovery in the postgenomic era by estimating probabilities of activities like anti-inflammatory, antioxidant, and antiviral effects based on structure–activity relationships from large datasets, transforming vast data into meaningful knowledge [4]. In this review, such predictions guided interpretation of structure–activity trends across monopyrones, dipyrones, and arzanol analogues, identifying leads for dual mPGES-1/5-LO inhibition and low toxicity.

Literature Search Methodology

A comprehensive literature review was performed to identify published research articles reporting the synthesis of naturally occurring phloroglucinol α-pyrones isolated from *Helichrysum* species or their structural modification, as well as their synthetic analogues. The literature search was primarily conducted using Google Scholar as the electronic database. Combinations of keywords such as "*Helichrysum*", "alpha-pyrone", "α-pyrone", "phloroglucinol", and "synthesis" were employed. The retrieved records were subsequently screened manually for relevance. Original research articles describing the synthesis of phloroglucinol–α-pyrone derivatives from any *Helichrysum* species, as well as their

synthetic analogues, were included, together with studies reporting the biological activities of these compounds.

2. Materials and Methods

Computational Assessment of Biological Properties

In silico biological assessment was performed to the all phloroglucinol α-pyrones discussed in the synthetic section using the online provided free service PASS online (http://www.way2drug.com/passonline, accessed on 6 August 2025) [5]. The Prediction of Activity Spectra for Substances (PASS) is a computational tool designed to estimate the probable biological activity profiles of chemical compounds based on their structural representations in MOLfile or SDfile format. The platform encompasses a comprehensive list of over 4000 biological activity types, including pharmacotherapeutic effects (e.g., antiarrhythmic activity), mechanisms of biochemical action (e.g., cyclooxygenase-1 inhibition), toxicological properties (e.g., carcinogenicity), metabolic interactions (e.g., CYP3A4 inhibition), regulation of gene expression (e.g., inhibition of VEGF expression), and transporter-related behaviors (e.g., substrate of P-glycoprotein). PASS predictions are grounded in a robust knowledge base of structure–activity relationships (SARs) derived from more than one million compounds with experimentally validated biological activities. The method achieves an average prediction accuracy of approximately 96%, as evaluated using a leave-one-out cross-validation procedure across the entire PASS training dataset [5]. The program calculates the probable activity (P_a) and probable inactivity ($\mathbf{P_i}$) of a given compound, generating predictions regarding both its potential biological activities and its spectrum of adverse or toxic effects. The output is presented as a list of activity types, each accompanied by an estimated probability of being classified as "active" ($\mathbf{P_a}$) or "inactive" ($\mathbf{P_i}$). In typical cases, the values of P_a and P_i do not equal 1 simultaneously. Both parameters are expressed as probabilities on a continuous scale ranging from 0.000 to 1.000 [5].

3. Monopyrone Derivatives

Two α-pyrone derivatives were synthesized using β-keto ester and phloroglucinol-type precursors as part of an investigation into the structure–activity relationships of phloroglucinyl pyrones such as arzanol, a natural anti-inflammatory compound found in *Helichrysum italicum*.

One of the synthesized compounds, 6-ethyl-4-hydroxy-5-methyl-α-pyrone **1s** ($C_8H_{10}O_3$; exact mass 154.063), (Figure 1) was obtained through a two-step synthetic sequence. Initially, a β-keto ester intermediate was generated by base-promoted condensation of ethyl 3-oxopentanoate with ethyl propionate, using sodium hydride (NaH) and *n*-butyllithium (*n*-BuLi) in tetrahydrofuran (THF) at low temperature. This afforded ethyl 4-methyl-3,5-dioxoheptanoate in good yield (62%). In the subsequent step, the intermediate underwent cyclodehydration with polyphosphoric acid (PPA) at 120 °C to afford the desired α-pyrone **1s** in 74% yield [2] (Scheme 1).

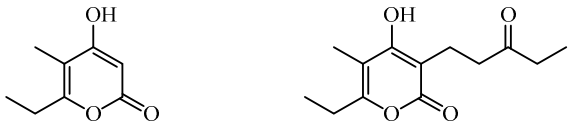

6-Ethyl-4-hydroxy-5-methyl-α-pyrone (1s) **Helipyrone ketone (2s)**

Figure 1. Structural formulas of **1s** and **2s**.

In contrast, helipyrone ketone **2s** ($C_{13}H_{18}O_4$; exact mass 238.1205) was obtained via mild oxidative transformation of helipyrone **6** using aqueous sodium carbonate under reflux conditions, followed by acid quenching and silica gel purification. The reaction

proceeds through decarboxylation and cleavage of the chelated enol system, yielding the ketone in 60% isolated yield as colorless crystals with a melting point of 75 °C and a UV maximum at 295 nm (log ε = 3.88) [6] (Scheme 2).

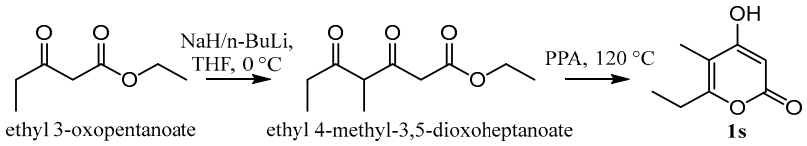

Scheme 1. Synthesis of 6-Ethyl-4-hydroxy-5-methyl-α-pyrone **1s**.

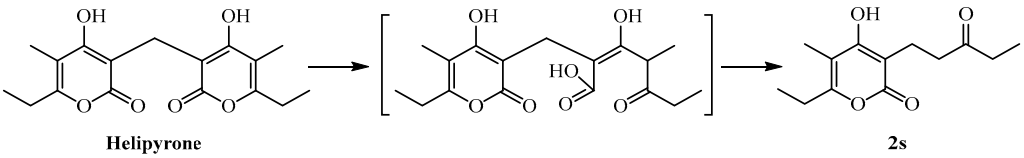

Scheme 2. Synthesis of 6-ethyl-4-hydroxy-5-methyl-3-(3-oxopentyl)-2H-pyran-2-one **2s**.

Helipyrone (**6**) has been reported to exhibit moderate antiparasitic activity and limited selectivity toward mammalian cells. In axenic amastigotes of *Leishmania donovani*, the compound displayed antileishmanial activity with an IC_{50} value of 14.9 ± 3.1 μM, as determined by a colorimetric assay (100–0.001 $\mu g/mL^{-1}$). However, this activity was associated with relatively weak selectivity with selectivity index (SI) of 3.6 when compared to cytotoxicity in rat L6 myoblast cells (IC_{50} 54.3 ± 9.5 μM). Similarly, helipyrone (**6**) demonstrated antiplasmodial activity against the erythrocytic stages of *Plasmodium falciparum*, with an IC_{50} of 8.9 ± 1.2 μM in the same assay format, yielding a slightly improved but still modest SI of 5.4 versus L6 cells [7].

The cyclodehydration strategy using polyphosphoric acid provides a straightforward and reliable approach to α-pyrone construction, affording good isolated yields from readily available β-keto ester precursors. The methodology is operationally simple and tolerant of alkyl substitution on the pyrone ring. However, the requirement for strong acidic conditions and elevated temperatures may limit compatibility with acid-sensitive functional groups. Furthermore, the multistep preparation of β-keto ester intermediates reduces the overall synthetic efficiency, indicating that alternative catalytic or one-pot methodologies could further improve the sustainability of α-pyrone synthesis.

4. Dipyrone Derivatives

A series of dipyrone-type α-pyrone derivatives was synthesized via the homodimerization of 4-hydroxypyrones, using either 6-methyl-4-hydroxypyrone **3s**–**6s** (Scheme 3) or 6-ethyl-4-hydroxy-5-methyl-α-pyrone **8s**–**10s** (Scheme 4) as nucleophilic substrates. These reactions were carried out under mild conditions and involved condensation with aldehydes as a methylene-bridging agent, yielding a structurally diverse array of symmetrical bis-α-pyrone compounds [2].

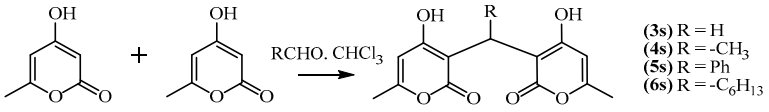

Scheme 3. Synthesis of compounds **3s**–**6s**.

The resulting bis-α-pyrones feature two identical pyrone moieties bridged through a central methylene group, forming rigid and symmetrical frameworks. This synthetic strategy provides an efficient and scalable route to pyrone dimers that are structurally

related to natural products such as arzanol and helipyrone, and may serve as valuable scaffolds for further biological or medicinal exploration.

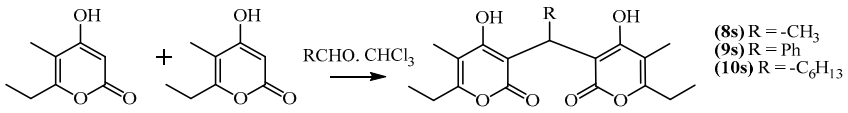

Scheme 4. Synthesis of compounds **8s–10s**.

The first group of compounds consisted of symmetrical bis-α-pyrone derivatives, synthesized via aldehyde-mediated homodimerization of 4-hydroxy-6-methyl-α-pyrone derivatives. These reactions yielded a structurally diverse set of dimeric pyrones, including: 3,3′-methylenebis(4-hydroxy-6-methyl-2H-pyran-2-one), **3s** $C_{13}H_{12}O_6$, exact mass 264.0634; 63% yield, 3,3′-(ethane-1,1-diyl)bis(4-hydroxy-6-methyl-2H-pyran-2-one), **4s**, $C_{14}H_{14}O_6$, exact mass 278.079; 60% yield, 6-diethyl-1′-phenyl-6-methylhelipyrone, **5s**, $C_{19}H_{16}O_6$, exact mass 340.0947; 55% yield, and 6-diethyl-1′-hexyl-6-methylhelipyrone, **6s**, $C_{19}H_{24}O_6$, exact mass 348.1573; 68% yield (Scheme 3).

The second group, including 1′-methylhelipyrone **8s**, $C_{18}H_{22}O_6$, exact mass 334.1416; 65% yield, 1′-phenylhelipyrone **9s**, $C_{23}H_{24}O_6$, exact mass 396.1573; 52% yield, and 1′-hexylhelipyrone **10s**, $C_{23}H_{32}O_6$, exact mass 404.2199; 66% yield, were synthesized using 6-ethyl-4-hydroxy-5-methyl-α-pyrone **1s** as the precursor (Scheme 4).

All derivatives were prepared by analogous procedures: condensation of the respective α-pyrone core with the appropriate aldehyde under the same synthetic conditions, followed by purification. For example, both 6-diethyl-1′-hexyl-6-methylhelipyrone **6s** and 1′-hexylhelipyrone **10s** were obtained by condensation of hexanal with either 4-hydroxy-6-methyl-α-pyrone or 6-ethyl-4-hydroxy-5-methyl-α-pyrone, respectively, and isolated after similar work-up and purification protocols.

These homodimerization reactions provide an efficient access to bis-α-pyrone structures. From a medicinal chemistry perspective, the resulting dimers combine a low degree of structural complexity with high synthetic accessibility and defined points for substitution.

The aldehyde-mediated homodimerization strategy represents a simple and modular approach for preparing symmetrical dipyrone derivatives. One of its principal advantages is the broad availability of aldehydes, allowing rapid diversification of substituents without modifying the pyrone core. Nevertheless, the methodology is inherently limited to symmetrical dimers and therefore cannot provide the structural diversity accessible through heterodimerization strategies. In addition, moderate isolated yields suggest that competing oligomerization or side reactions may reduce synthetic efficiency.

All synthesized dipyrones were evaluated for inhibition of microsomal prostaglandin E_2 synthase-1 (mPGES-1) and 5-lipoxygenase (5-LO), key targets in inflammatory signaling. Most compounds exhibited weak or negligible inhibition (IC_{50} for mPGES-1 > 67 μM; IC_{50} for 5-LO > 56 μM), except for 1′-hexylhelipyrone **10s**, which showed moderate dual inhibitory activity (mPGES-1 IC_{50} 0.84 μM; 5-LO IC_{50} 56 μM), with a pronounced selectivity for mPGES-1 [2].

5. Synthesis of Arzanol

Arzanol **10** ($C_{22}H_{26}O_7$; exact mass 402.1678 Da), a natural phloroglucinyl α-pyrone derivative with notable anti-inflammatory and antioxidant properties, has been the subject of significant synthetic interest due to its unique heterodimeric structure and therapeutic potential [8–11].

Arzanol features a 2,4,6-trihydroxyacetophenone unit linked via a central methylene bridge to a 6-ethyl-4-hydroxy-5-methyl-α-pyrone **1s**, forming a core structure similar to that of helipyrone **6**.

Arzanol has been successfully isolated from two Mediterranean *Helichrysum* species: *H. italicum* (Roth) G. Don subsp. *microphyllum* [1,3,12–15] and *H. stoechas* (L.) Moench [6], where yields ranged from 0.002% to as high as 0.48% *w*/*w*.

In the study by Minassi et al. [2], arzanol was synthesized via two complementary procedures, both relying on a carba-Betti-type multicomponent condensation but differing in the source of the methylene linker used during the key coupling step. In Procedure A, the authors employed paraformaldehyde as the methylene donor in the presence of tetrabutylammonium fluoride (TBAF, 1 M in THF) as a Lewis base catalyst. The reaction was carried out in chloroform and stirred at 40 °C for 16 h under mild conditions. Upon completion, the reaction mixture was quenched with water, extracted with organic solvent, and the crude product was purified by silica gel chromatography using a mixture of petroleum ether and acetic acid as the eluent. This protocol yielded arzanol, corresponding to a 61% yield, with full characterization by NMR and mass spectrometry confirming the expected structure [2] (Scheme 5).

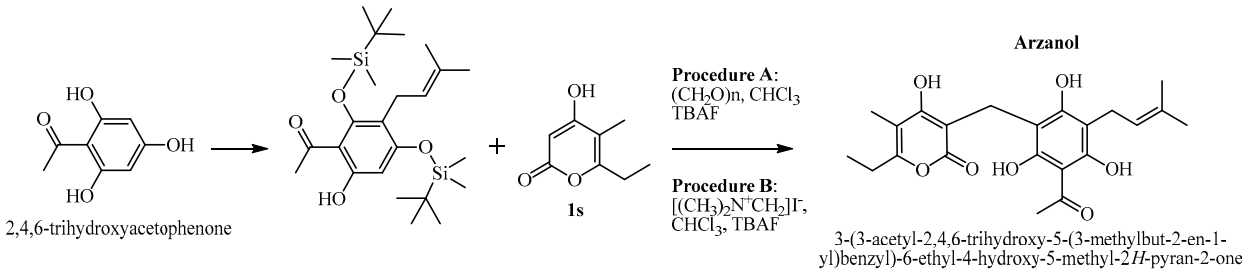

Scheme 5. Synthesis of arzanol **10**.

This method is noteworthy for its efficiency, functional group tolerance, and operational simplicity, allowing for the selective formation of the arzanol scaffold without the need for protecting groups or transition metal catalysts. The modularity of the approach also permits substitution at various positions on the pyrone or phloroglucinol ring, facilitating the synthesis of structurally diverse analogues for structure–activity relationship (SAR) studies.

Importantly, the successful synthesis of arzanol using paraformaldehyde supports its biosynthetic plausibility, as such methylene donors are likely intermediates in plant-derived coupling reactions arzanol [2].

In Procedure B, the synthesis of arzanol **10** was achieved using Eschenmoser's salt (*N*,*N*-dimethylmethyleneiminium iodide) as an alternative methylene donor, under reaction conditions identical to those used in Procedure A. Specifically, 6-ethyl-4-hydroxy-5-methyl-α-pyrone and phloracetophenone were reacted in the presence of TBAF (1 M in THF) in chloroform, and the mixture was stirred at 40 °C for 16 h. The reaction was then quenched with water, extracted with organic solvent, and purified by silica gel chromatography using a petroleum ether/acetic acid eluent system.

This approach resulted in the isolation of arzanol, corresponding to a 65% yield, slightly higher than that obtained using paraformaldehyde. The structure of the product was confirmed by NMR and MS data, and found to be identical to that obtained in Procedure A.

The use of Eschenmoser's salt presents several advantages: as a preformed, soluble methylene equivalent, it offers improved solubility and reactivity under the mild, non-acidic conditions of the coupling reaction. Its application in this synthesis exemplifies the

versatility of the methylene bridging strategy for accessing the central alkylidene linkage in the arzanol scaffold. Moreover, this method avoids the need to generate formaldehyde in situ and may offer greater reproducibility and cleaner reaction profiles in complex or sensitive substrates.

Thus, Procedure B complements Procedure A by offering an alternative, equally effective route to arzanol, underscoring the modularity and practicality of the synthetic approach developed by Minassi and co-workers for accessing natural and bioinspired phloroglucinyl-α-pyrone hybrids (Scheme 5).

Compared with paraformaldehyde, Eschenmoser's salt provides a more reactive and soluble methylene donor, resulting in slightly improved yields and potentially improved reproducibility. However, paraformaldehyde remains considerably less expensive and more readily available, making it attractive for larger-scale synthesis. Both methodologies avoid transition-metal catalysis and proceed under relatively mild conditions, although the prolonged reaction time (16 h) and chromatographic purification may reduce their practical scalability.

Arzanol demonstrates diverse pharmacological properties with significant therapeutic potential. As a potent anti-inflammatory agent, it inhibits NF-κB signaling (IC_{50} = 12 μM) and functions as a dual inhibitor of mPGES-1 (IC_{50} = 0.4 μM) and 5-LOX (IC_{50} = 3.1 μM), effectively suppressing pro-inflammatory cytokines and prostaglandin production [1,16]. Its antioxidant activity provides dose-dependent protection against lipid peroxidation in LDL and cellular models, with efficacy comparable to established antioxidants like α-tocopherol [11]. Arzanol exhibits cytoprotective effects in keratinocytes and neuronal cells against oxidative stress, preventing apoptosis and maintaining mitochondrial integrity [9,10]. Antimicrobial screening revealed selective antibacterial activity against drug-resistant *Staphylococcus aureus* strains (MIC = 1–4 μg/mL) [3]. In neurobehavioral studies, arzanol-containing extracts produced anxiolytic and antidepressant effects comparable to diazepam and amitriptyline, respectively, without impairing locomotor or memory function [17]. The compound shows selective cytotoxicity against cancer cells, particularly Caco-2 colon cancer cells, while sparing normal cells at concentrations below 100 μM [15].

6. Phloroacetophenone Alpha-Pyrone Derivatives

A set of arzanol analogues was synthesized by the condensation of phloracetophenone with either 6-methyl-4-hydroxypyrone **11s**–**14s**, Scheme 6 or 6-ethyl-4-hydroxy-5-methyl-α-pyrone **17s**–**19s**, Scheme 7, using a range of aldehydes as the linking agents. The reactions were catalyzed by tetrabutylammonium fluoride (TBAF) in chloroform at 40 °C, typically proceeding for 16 h. After completion, the mixtures were subjected to purification on silica gel, using acidic petroleum ether as the eluent [2].

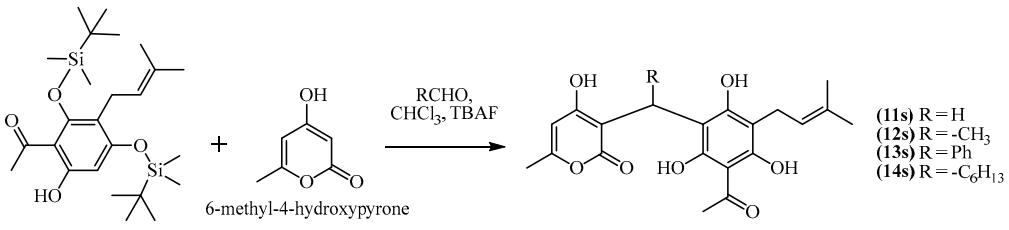

Scheme 6. Synthesis of arzanol derivatives **11s**–**14s**.

Compounds 6-diethyl-5,5,6-trimethylarzanol **11s**, $C_{20}H_{22}O_7$; exact mass 374.1365, 58% yield, 6-diethyl-1′,5,5,6-tetramethylarzanol **12s**, $C_{21}H_{24}O_7$; exact mass 388.1522, 55% yield, 6-diethyl-5,5,6-trimethyl-1′-phenylarzanol **13s**, $C_{26}H_{26}O_7$; exact mass 450.1678, 30% yield,

and 6-diethyl-1′-hexyl-5,5,6-trimethylarzanol **14s**, $C_{26}H_{34}O_7$; exact mass 458.2304, 40% yield were prepared using 6-methyl-4-hydroxypyrone as the pyrone core (Scheme 6).

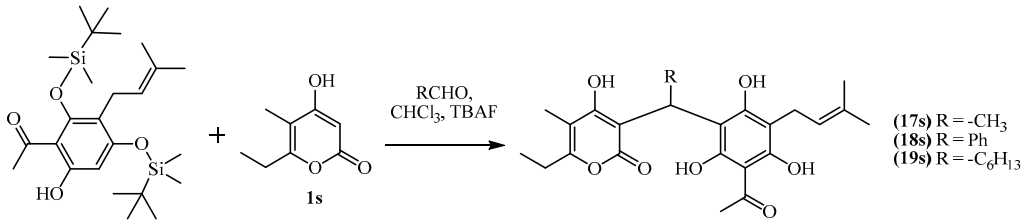

Scheme 7. Synthesis of 1′-methylarzanol **17s**, 1′-phenylarzanol **18s**, and 1′-hexylarzanol **19c**.

In contrast, 1′-methylarzanol **17s**, $C_{23}H_{28}O_7$; exact mass 416.1835, 68% yield, 1′-phenylarzanol **18s**, $C_{28}H_{30}O_7$; exact mass 478.1991, 31% yield, and 1′-hexylarzanol **19s**, $C_{28}H_{38}O_7$; exact mass 486.2617, 48% yield were synthesized from 6-ethyl-4-hydroxy-5-methyl-α-pyrone [2] (Scheme 7).

This methodology enabled the selective formation of heterodimeric products such as arzanol and allowed the straightforward generation of a diverse array of analogues for subsequent structure–activity relationship studies. Both aliphatic and aromatic aldehydes were explored; while aliphatic aldehydes afforded better yields of the desired products, aromatic aldehydes often required conversion to their iminium equivalents to achieve efficient heterodimerization. Tetrabutylammonium fluoride (TBAF) served as a catalyst in the synthesis of arzanol analogues, promoting the reaction via fluoride-induced desilylation of the phloracetophenone derivative. This activation step enhanced the nucleophilicity of the phenolic component, enabling efficient heterodimerization under mild, neutral conditions without compromising the acid- and base-labile products.

Compared with the synthesis of symmetrical dipyrone derivatives, the TBAF-mediated heterodimerization provides substantially greater structural diversity, enabling independent modification of both the phloroglucinol and α-pyrone fragments. This modularity is particularly advantageous for medicinal chemistry, as it facilitates rapid optimization of biological activity through systematic variation of substituents. The observed enhancement in anti-inflammatory activity of the hexyl-substituted analogues illustrates the effectiveness of this approach for SAR exploration. Despite these advantages, the methodology still relies on relatively long reaction times, moderate isolated yields for several derivatives, and chromatographic purification, highlighting opportunities for future optimization through more sustainable catalytic systems, one-pot protocols, or greener reaction media. Thus, this strategy represents one of the most versatile synthetic routes reported for accessing arzanol-inspired analogues.

All compounds were evaluated for inhibition of mPGES-1 and 5-lipoxygenase (5-LO). Most analogues displayed low-micromolar activity against mPGES-1 (IC_{50} 0.2–2.4 μM) and micromolar activity against 5-LO (IC_{50} 1.2–9.5 μM), with a clear preference for mPGES-1. The most potent inhibitors were 6-diethyl-1′-hexyl-5,5,6-trimethylarzanol **14s** and 1′-hexylarzanol **19s**, with mPGES-1 IC_{50} values of 0.2 μM and 0.3 μM, respectively [2].

In antibacterial assays, 6-diethyl-5,5,6-trimethylarzanol **11s** showed strong activity against MDR Staphylococcus aureus (MIC 1–2 $\mu g/mL^{-1}$), while 6-diethyl-1′-hexyl-5,5,6-trimethylarzanol **14s** and 1′-hexylarzanol **19s** demonstrated moderate to good activity (MIC 4–16 $\mu g/mL^{-1}$). 6-Diethyl-1′,5,5,6-tetramethylarzanol **12s** and 1′-methylarzanol **17s** exhibited only weak antibacterial activity (MIC $\geq$ 32 $\mu g/mL^{-1}$). These findings emphasize the impact of both pyrone substitution pattern and side-chain variation on the anti-inflammatory and antibacterial profiles of synthetic Arzanol analogues [2,3].

7. Cyclization of Arzanol to Cycloarzanol A and B

Two cyclized derivatives of arzanol, cycloarzanol A **15s** and cycloarzanol B **16s**, both sharing the molecular formula $C_{22}H_{26}O_7$ (exact mass 402.1678 Da), were synthesized through acid-catalyzed intramolecular cyclization of the parent compound Arzanol [1].

As described [1], treatment of arzanol with trifluoroacetic acid (TFA) in an appropriate solvent system induced selective cyclization of the phloroglucinol and methylene-bridged α-pyrone moieties, giving rise to the tricyclic structures of cycloarzanol A and cycloarzanol B. The reaction was likely driven by the electron-rich nature of the phloroglucinol ring and the proximity of reactive centers, allowing for electrophilic aromatic substitution-type ring closure.

The two isomers differ in the regiochemistry of the cyclization, possibly due to competing reaction pathways or conformational preferences of the arzanol scaffold [1].

Cycloarzanol A **15s** was synthesized via two distinct acid-catalyzed cyclization protocols, each promoting intramolecular ring closure of arzanol **10** to afford the tricyclic product. In the first approach, referred to as the $CeCl_3$ method, arzanol was treated with cerium (III) chloride in anhydrous tetrahydrofuran (THF) and allowed to stir at room temperature for one week. This mild Lewis acid-mediated transformation yielded cycloarzanol A in 28% yield, indicating moderate efficiency under prolonged reaction conditions. The second method employed a more classical Brønsted acid approach, wherein arzanol was exposed to methanolic hydrochloric acid, generated in situ from thionyl chloride ($SOCl_2$) and methanol. The reaction was initiated at 0 °C for one hour, followed by stirring at room temperature overnight, leading to the formation of cycloarzanol A in 29% yield. This protocol offers a shorter reaction time compared to the $CeCl_3$ route, albeit with similar efficiency. Both methods likely proceed through electrophilic activation of the benzylic methylene bridge, facilitating intramolecular aromatic substitution and cyclization onto the phloroglucinol ring. The formation of cycloarzanol A via two chemically distinct yet convergent pathways underscores the versatility of the arzanol scaffold and its potential for structural diversification through mild acid-promoted transformations [1].

Cycloarzanol B **16s** was obtained as a minor cyclization product under the same conditions employed for the synthesis of cycloarzanol A **15s**, reflecting the formation of a regioisomeric benzopyran framework. When arzanol **10** was subjected to cerium (III) chloride ($CeCl_3$) in dry THF at room temperature for one week, cycloarzanol B was isolated in 18% yield. Alternatively, the methanolic HCl protocol, using hydrochloric acid generated in situ from $SOCl_2$ and methanol, afforded cycloarzanol B in only 6% yield following a similar sequence of cooling to 0 °C and subsequent overnight stirring at ambient temperature [1].

Both cycloarzanol A **15s** and cycloarzanol B **16s** were purified by silica gel column chromatography, employing a petroleum ether/ethyl acetate (95:5) solvent system. The relatively low yields of **16s** in both methods suggest a less favorable cyclization pathway, likely influenced by regioelectronic and steric factors governing the orientation of the intramolecular electrophilic aromatic substitution.

In contrast to these cyclization products, methylation of arzanol using trimethylsilyldiazomethane led to the formation of the corresponding *O*-methyl derivative, identified as 3-(3-acetyl-2,4,6-trihydroxy-5-(3-methylbut-2-en-1-yl)benzyl)-6-ethyl-2-methoxy-5 -methyl-4H-pyran-4-one. This reaction proceeded cleanly without inducing cyclization, indicating that methylation effectively blocks the phenolic hydroxyl groups necessary for ring closure.

Under acidic conditions, however, cyclization is favored, and a separable mixture of cycloarzanol A **15s** and cycloarzanol B **16s** is formed (Scheme 8). These products arise through an intramolecular electrophilic attack of the prenyl side chain onto the ortho-positioned phenolic hydroxyls of the phloroglucinol moiety, yielding structurally distinct benzopyran frameworks. This transformation not only exemplifies the reactivity of arzanol

under mildly acidic conditions but also provides synthetic access to complex tricyclic architectures relevant to natural product analog development [1].

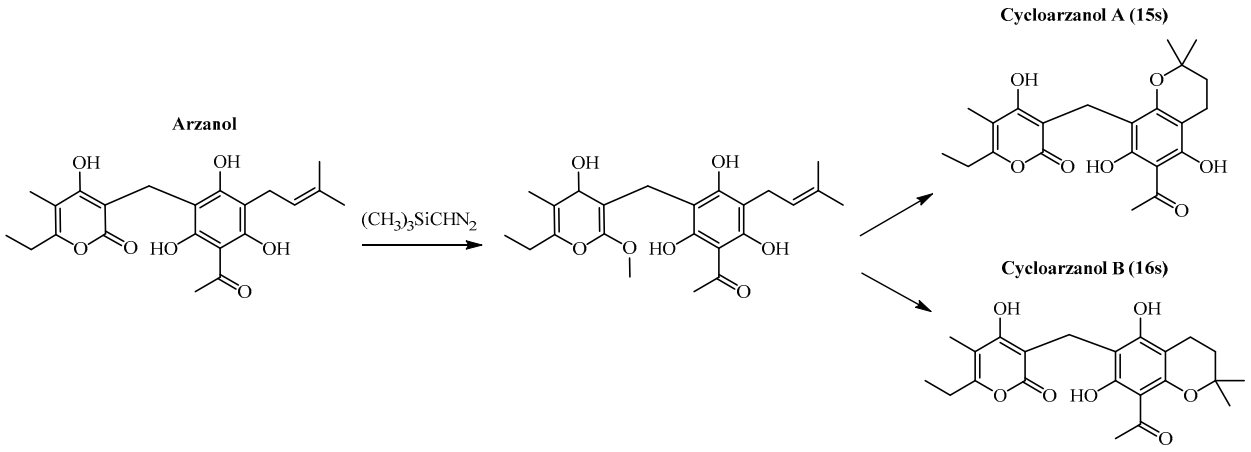

Scheme 8. Synthesis of cycloarzanol A and B.

The acid-promoted cyclization of arzanol provides an elegant biomimetic strategy for accessing structurally complex tricyclic derivatives through a single intramolecular transformation. The ability to generate two distinct cyclized products from a common precursor highlights the inherent structural versatility of the arzanol scaffold and demonstrates the potential of this approach for expanding the chemical diversity of phloroglucinol–α-pyrone derivatives. However, the relatively low isolated yields (6–29%) indicate that the cyclization process is not highly efficient under the reported conditions, likely due to competing reaction pathways and the formation of regioisomeric products. In addition, the prolonged reaction time required for the $CeCl_3$-mediated protocol and the need for chromatographic purification may limit the practical scalability of these methods. Nevertheless, the successful construction of complex benzopyran frameworks under relatively mild conditions illustrates the synthetic value of this transformation and provides a foundation for future optimization through alternative catalysts, greener reaction media, or more selective cyclization strategies.

Cycloarzanol A **15s** showed limited antibacterial activity against multidrug-resistant *Staphylococcus aureus* isolates with MICs of 32 μg/mL against ATCC 25923 and RN4220, 128 μg/mL against SA1199B, XU212, and EMRSA-15, and >128 μg/mL against EMRSA-16. Cycloarzanol B was inactive against all tested strains (MIC > 128 μg/mL) [1].

8. Methyl Ether Derivatives

Auricepyrone dimethyl ether **23s**, $C_{26}H_{34}O_7$; and 23-methylauricepyrone dimethyl ether **24s**, $C_{27}H_{36}O_7$, both obtained in quantitative yield were prepared by exhaustive methylation of a mixture of auricepyrone **19** and 23-methylauricepyrone **20** (20 mg total). This transformation was achieved using an excess of diazomethane in dry diethyl ether at room temperature (Scheme 9).

Following the reaction, the solvent was removed under reduced pressure, and the crude products were purified by silica gel chromatography (eluent: ether/petroleum ether, 1:1), affording both compounds as colorless oils. The original study did not report any biological activity data for either auricepyrone dimethyl ether or its 23-methyl analogue [18].

The exhaustive methylation of auricepyrone derivatives represents a highly efficient post-synthetic modification, proceeding in quantitative yields under mild reaction conditions. This transformation provides a convenient strategy for modulating the physicochemical properties of phloroglucinol–α-pyrone derivatives by reducing the number of

free phenolic hydroxyl groups, thereby increasing lipophilicity and potentially improving membrane permeability and metabolic stability. From a synthetic perspective, methylation also serves as a valuable tool for protecting phenolic functionalities during multistep synthesis and for probing the contribution of hydroxyl groups to biological activity. However, the use of diazomethane presents significant practical and safety limitations due to its high toxicity and explosive nature, restricting its applicability on a larger scale. Consequently, the development of safer methylating reagents or catalytic methylation protocols would further enhance the sustainability and practical utility of this transformation in future synthetic studies.

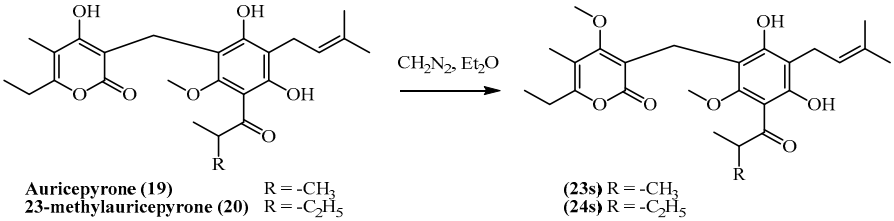

Scheme 9. Synthesis of auricepyrone dimethyl ether **23s** and 23-methylauricepyrone dimethyl ether **24s**.

9. Acetyl Derivatives

Among the most common modifications are acetylation of the phenolic hydroxyl groups. Acetyl derivatives of phloroglucinol–α-pyrones were obtained through mild reactions with acetic anhydride, which selectively protect hydroxyl groups and reduce overall polarity. These transformations are not only useful for structural characterization and stability enhancement, but also serve as key intermediates in synthetic sequences, including methylation, cyclization, or multicomponent coupling reactions. Additionally, acetylation can modulate biological activity by altering hydrogen-bonding patterns and improving membrane permeability, making these derivatives important tools in both natural product chemistry and medicinal chemistry research.

Acetylations have been carried out on dipyrones: helipyrone diacetate **7s**; 3-prenyl PG: arzanol tetraacetate **20s**, 6-*O*-desmethylauricepyrone tetraacetate **21s**, 23-methyl-6-*O*-desmethylauricepyrone tetraacetate **22s**, auricepyrone triacetate **25s**, methylauricepyrone triacetate **26s**; benzopyrane: 22,22-dimethylitalipyrone triacetate **27s**, 22-methyl-22-ethylitalipyrone triacetate **28s**; hetero-trimer PGs: 23-methylitalidipyrone tetraacetate **29s**, italidipyrone tetraacetate **30s** (Figure 2).

The synthesis of acetate derivatives consistently utilized acetic anhydride as the acetylating reagent, applying two primary methodological approaches. Predominantly, acetylation reactions were performed in chloroform solvent under an inert nitrogen atmosphere to minimize side reactions and degradation. These reactions incorporated catalytic quantities of 4-pyrrolidinopyridine, which served as an efficient acyl transfer catalyst, thereby facilitating the acetylation process under mild conditions. This catalytic system enhance the reaction rates and yields, and also improves selectivity, allowing for the controlled acetylation of polyhydroxylated phloroglucinol derivatives [6].

The acetylation reactions were generally conducted under reflux conditions for a duration of 2 to 3 h. Upon completion, the reaction mixtures were subjected to solvent removal, and the residues were purified by silica gel column chromatography using moderately non-polar solvent systems, such as cyclohexane/ethyl acetate or petroleum ether/diethyl ether mixtures. Alternatively, protocols [6,19] have been reported wherein pyridine served both as the solvent and as a base catalyst. In these procedures, the reactions were allowed to proceed at ambient temperature for prolonged periods, often extending up to 24 h. The

resulting crude products were frequently purified by direct crystallization, obviating the need for chromatographic separation. These varied methodologies provide flexibility in optimizing acetylation conditions depending on substrate sensitivity and desired purity.

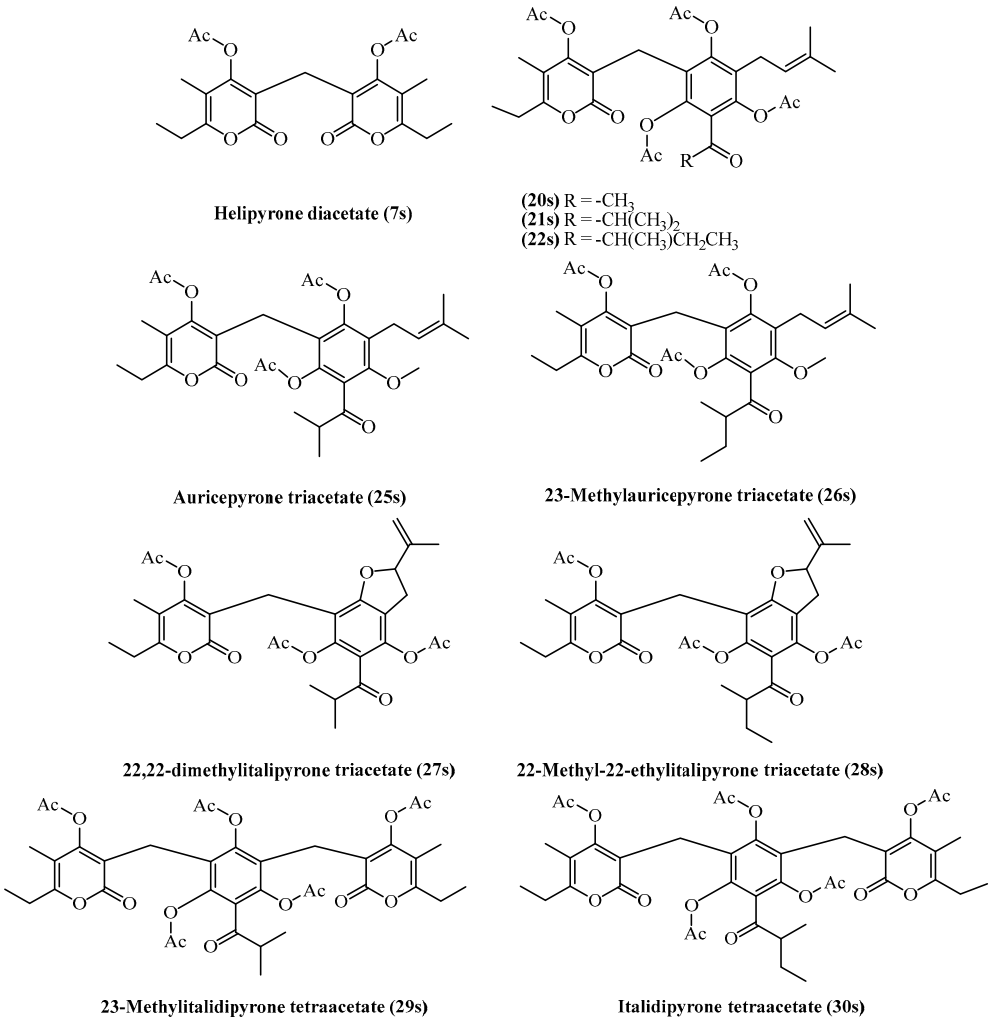

Figure 2. Structural formulas of compounds acetyl derivatives of phloroglucinol–*α*-pyrones.

The acetylation reactions proceeded with generally high efficiency. For example, the acetylation of 6-*O*-desmethylauricepyrone and its 23-methyl analogue yielded the corresponding tetraacetylated derivatives in a combined yield of approximately 83%, although the products were obtained as an inseparable mixture under the reported conditions [6]. Similarly, the diacetylation of italidipyrone **43** and 23-methyl-italidipyrone **44** afforded a combined mixture of diacetylated products in 72% yield [6]. In contrast to the tetraacetylated derivatives, this product mixture could be successfully separated by crystallization, allowing for individual characterization of the components. The triacetate derivatives, auricepyrone triacetate **25s**, $C_{31}H_{38}O_{10}$; exact mass 570.2465 Da and 23-methylauricepyrone triacetate **26s**, $C_{32}H_{40}O_{10}$; exact mass 584.2622 Da, were synthesized via acetylation of the corresponding natural products, auricepyrone **19** and 23-methylauricepyrone **20**. The reaction was performed by refluxing in chloroform in the presence of 4-pyrrolidinopyridine as a nucleophilic catalyst and acetic anhydride as the acetylating agent, following the procedure described by Bohlmann [18]. After concentration and column chromatography (ether: petroleum ether 3:1), the triacetates were isolated together as a colourless oil in quantitative yield. No biological activity data were reported for either compound [18].

The acetylation conditions employed proved compatible with a range of substrates bearing multiple hydroxyl functionalities. No biological evaluations were reported for any of the acetylated compounds, suggesting that their synthesis was likely intended for purposes such as structural confirmation for NMR.

Acetylation represents one of the most straightforward and efficient post-synthetic modifications of phloroglucinol–α-pyrone derivatives, generally proceeding in excellent to quantitative yields under mild reaction conditions. Besides serving as a convenient protecting-group strategy for phenolic hydroxyl groups, acetylation alters the physicochemical properties of the molecules by increasing their lipophilicity and reducing hydrogen-bonding capacity, which may influence membrane permeability and pharmacokinetic behavior. From a synthetic perspective, the broad functional-group tolerance and operational simplicity of this transformation make it particularly useful for the preparation of intermediates in multistep synthetic sequences and for investigating structure–activity relationships. Nevertheless, acetylation does not introduce new molecular complexity and its direct impact on biological activity remains highly dependent on the specific molecular scaffold. Consequently, future studies should focus on evaluating the biological significance of acetylated derivatives and exploring more selective or environmentally benign acylation methodologies that further improve the sustainability of these transformations.

10. Unified Retrosynthetic Approaches Toward *Helichrysum* Phloroglucinol–Pyrone

Helichrysum benzofuranes are a small group of phloroglucinol-derived natural products with a substituted 2-vinyl-2,3-dihydrobenzofuran core. This family—including italipyrone **35a** and its alkylated homologues **35b–c**—has been isolated in low yield from *Helichrysum* species across Europe, Turkey, and South Africa, differing mainly in the acyl substituent. No total synthesis has been reported, so we propose a convergent retrosynthetic strategy built on literature precedent.

As outlined in Scheme 10, benzofuran intermediate **32** could be accessed from acylphloroglucinol derivative **31** via a modified Nickl cyclization [20]. The undesired ortho-fused isomer **33** forms in ~1:1 ratio but is readily separated by chromatography. Compound **31** itself is readily obtained by a classical Fries rearrangement of commercially available phloroglucinol. Silylation of both phenolic groups in **32** gives intermediate **34**, which may then couple with pyronoid fragment **1s** (Scheme 1) via Carba-Betti alkylidene heterodimerization, analogous to Minassi et al.'s arzanol synthesis [2,21]. This coupling is proposed as the final step, since 4-hydroxy-2-pyrones are prone to competing homoalkylidene dimerization [21]. Varying the acyl substituent (R) would thus give unified access to italipyrone and its natural analogues.

Based on a retrosynthetic approach, we propose a unified synthetic strategy for accessing 2-vinyl-2,3-dihydrobenzofuran phloroglucinol derivatives **32** through an intramolecular 5-exo-trig Tsuji–Trost allylic cyclization (Scheme 11). In this approach, the key allylic precursor **31a** is generated by phenolic prenylation [22] using (E)-4-bromo-2-methylbut-2-en-1-yl acetate, which can be readily prepared in three steps according to the procedure reported by Wei et al. [23]. The resulting prenylated phloroglucinol derivatives **31a** serve as substrates for a Pd-catalyzed intramolecular allylic substitution, where the phenoxide oxygen attacks the π-allyl palladium intermediate through a 5-exo-trig pathway to furnish the characteristic 2-vinyldihydrobenzofuran framework. It remains to be established experimentally whether this route improves on the ~1:1 mixture of regioisomers **32** vs. **33** obtained via the classical Nickl cyclization (Scheme 10). Furthermore, the proposed strategy offers the attractive possibility of asymmetric synthesis. Given the broad range of highly enantioselective Pd-catalyzed Tsuji–Trost allylic substitutions reported in the literature [24],

the use of suitable chiral phosphine ligands could potentially enable stereocontrolled cyclization, providing access to either enantiomer of these natural products from the same achiral precursor.

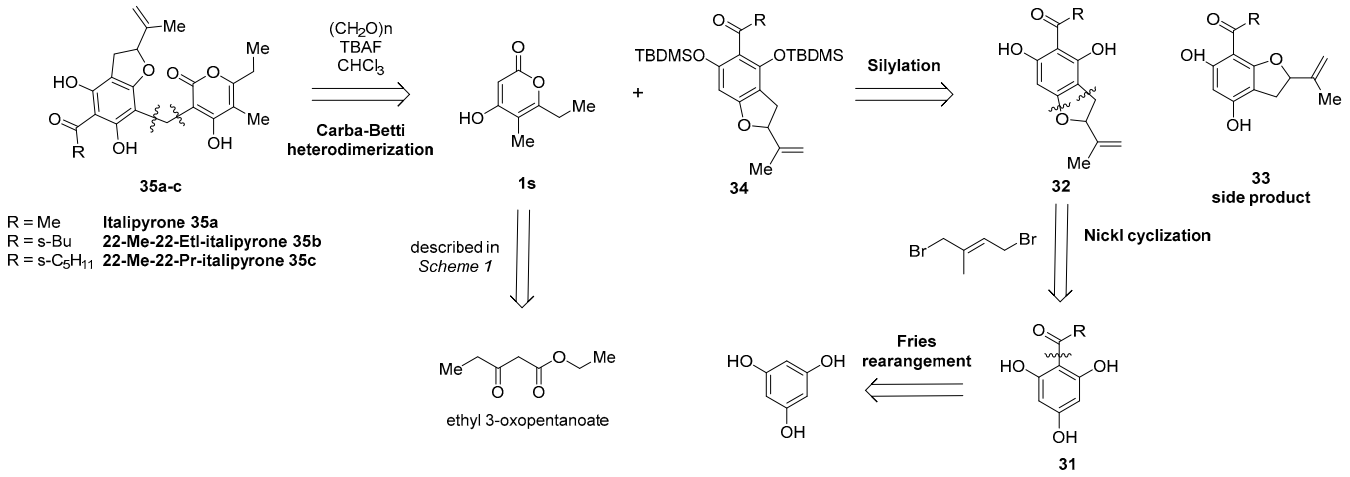

Scheme 10. Proposed retrosynthetic analysis of italipyrone-type benzofurane–2-pyrone heterodimers [2,21,22].

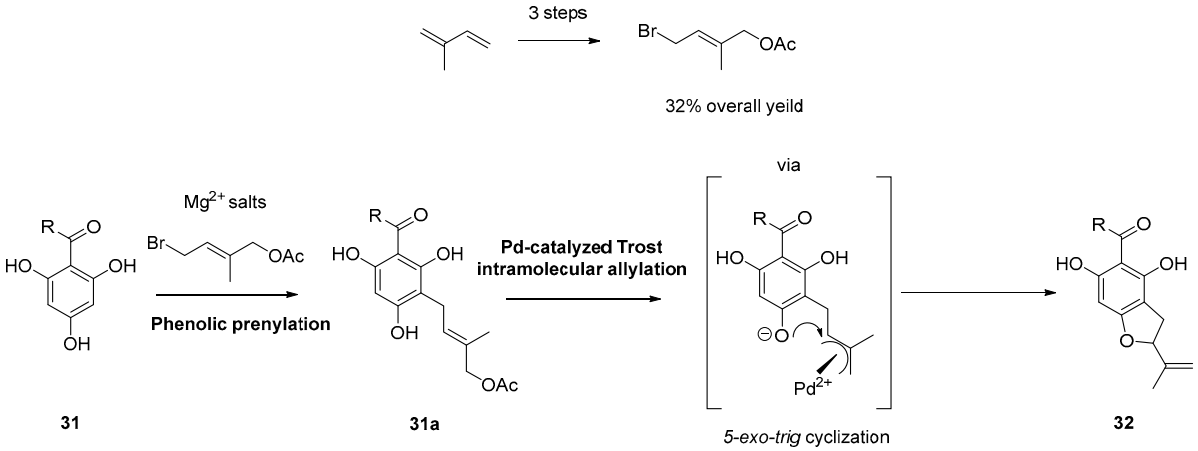

Scheme 11. Novel strategy for constructing 2-vinyl-2,3-dihydrobenzofurans [22,23].

This strategy establishes a direct retrosynthetic link between prenylated polyphenols and the corresponding benzofuran natural products and, to the best of our knowledge, represents the first proposal to access this class of compounds through an intramolecular Pd-catalyzed 5-exo-trig Tsuji–Trost allylic cyclization.

In contrast to the benzofuran derivatives, the benzopyrane-type metabolites possess a fused chromene framework linked to the pyronoid fragment. Representative members of this subclass include isobutyryl-helichromenopyrone **38a** and sec-butyl-helichromenopyrone **38b**, isolated from South African *Helichrysum* species, where they again differ mainly in the nature of the acyl substituent. As outlined in Scheme 12, a similar retrosynthetic logic may be applied, again identifying the alkylidene linkage to the 4-hydroxy-2-pyrone moiety as the key strategic bond. Thus, target compounds **38a–b** may be disconnected into chromene intermediate **37** and pyronoid fragment **1s** through a Carba-Betti alkylidene heterodimerization strategy analogous to that described above [2,21]. Chromene intermediate **37** could potentially be obtained through oxidative cyclization of prenylated acylphloroglucinol derivative **36**, accessible from acylphloroglucinol precursor **31** via magnesium-mediated phenolic prenylation [22,25]. As in the benzofuran series,

variation of the acyl substituent (R group) could provide unified access to structurally related members of this subclass.

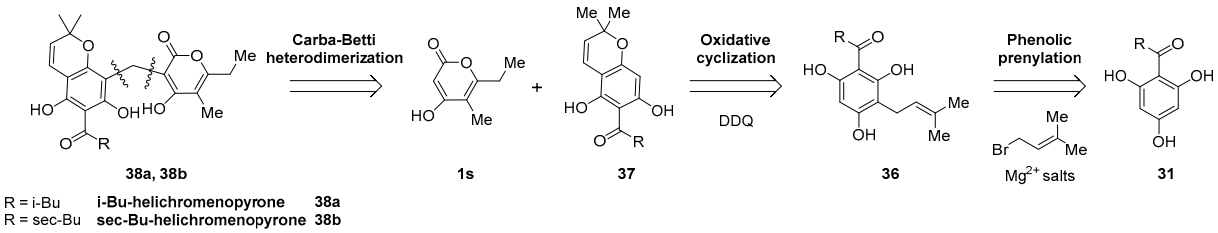

Scheme 12. Proposed retrosynthetic analysis of helichromenopyrone-type chromene heterodimers [2,22,25].

Cycloarzanol C represents a structurally distinct subclass of *Helichrysum* phloroglucinol metabolites featuring a fused chromane framework linked to an α-pyrone moiety through an alkylidene bridge. Nevertheless, the proposed retrosynthetic strategy shown in Scheme 13 retains the same convergent disconnection pattern observed for the benzofuran and chromene analogues, with late-stage construction of the alkylidene-linked heterodimer through a Carba-Betti-type transformation [2]. Retrosynthetically, the target compound may therefore be disconnected into chromane intermediate **39**. In this case, the chromane scaffold could plausibly arise directly from acylphloroglucinol precursor **31** through tandem conjugate addition and intramolecular cyclization, as described for related isoprenylated acetophenone derivatives [26]. Collectively, the retrosynthetic strategies outlined in Schemes 10–13 highlight a potentially unified synthetic approach toward structurally diverse *Helichrysum* phloroglucinol–pyrone heterodimers based on common acylphloroglucinol precursors and late-stage Carba-Betti alkylidene heterodimerization.

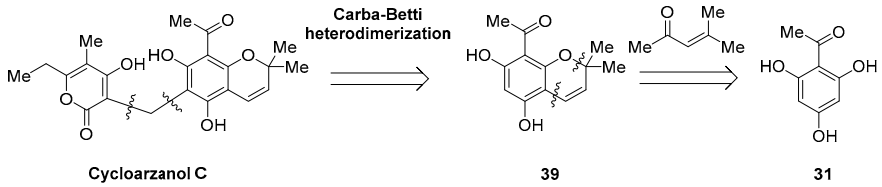

Scheme 13. Proposed retrosynthetic analysis of cycloarzanol C [2,26].

Systematic evaluation of the Nickl cyclization and Carba-Betti heterodimerization on the specific substitution patterns proposed here, ideally supported by DFT-level analysis of the competing homo- versus heterodimerization pathways, would help de-risk the routes before wet-lab implementation. Catalytic, enantioselective variants of the benzofuran-forming cyclizations would additionally allow access to the natural products in optically enriched form, which none of the current achiral routes can provide. Given the known instability of some methylene-donor reagents (e.g., Eschenmoser's salt-type iminium species) at scale, continuous-flow implementation of the alkylidene heterodimerization step could improve reproducibility and safety margins for larger-scale synthesis. More broadly, extending the acyl substituent (R group) scope beyond the simple alkyl chains modeled on the known natural products, to include aryl, heteroaryl, and fluorinated variants, would open a substantially larger chemical space for structure–activity exploration than is currently accessible from the isolated natural products alone. We consider these unresolved methodological questions, rather than the retrosynthetic logic itself, to be the principal barrier to realizing a unified synthetic platform for this compound family.

A caveat applies to the biological activity data compiled throughout this review. The present work is focused on the synthetic chemistry of *Helichrysum*-derived phloroglucinol

α-pyrones, and the biological activities are included as complementary context rather than as the primary subject of a systematic comparative assessment. Because these data were drawn from independent studies that employed different experimental protocols—including different enzyme sources, cell lines, bacterial strains, assay formats, incubation conditions, and reference standards—the reported potencies are not directly comparable across studies. For example, the mPGES-1 and 5-LO inhibition values originate largely from a single investigation and are therefore internally consistent, whereas the antibacterial and antiparasitic data were generated in separate laboratories using distinct methodologies. Consequently, absolute activity values should not be ranked across assays or sources, and the structure–activity observations noted herein are best regarded as qualitative trends that require confirmation under standardized conditions before firm comparative conclusions can be drawn.

The biological activity data were drawn from independent studies that employed different experimental protocols—including different enzyme sources, cell lines, bacterial strains, assay formats, incubation conditions, and reference standards—the re-ported potencies are not directly comparable across studies. Consequently, absolute activity values should not be ranked across assays or sources, and the structure–activity observations noted herein are best regarded as qualitative trends that require confirmation under standardized conditions before firm comparative conclusions can be drawn.

11. In Silico Biological Assessment

The PASS online platform is widely utilized by researchers across various disciplines to assess the potential biological activities of both newly synthesized compounds [25,27–29] and naturally derived substances [30–34]. Its ability to predict a broad spectrum of pharmacological, toxicological, and biochemical properties makes it valuable in the early stages of drug discovery and natural product research. A growing number of studies have employed PASS to evaluate bioactive compounds within complex plant or microbial extracts. This approach facilitates the prioritization of candidate molecules for further experimental validation and streamlines the development of novel therapeutic agents from both synthetic and natural origins [25,27–34].

The analysis of biological activity spectra using PASS online provides a probabilistic framework for predicting the pharmacological potential of chemical structures. By considering the ten most probable activities (P_a values) for each compound, it becomes possible to identify recurring mechanistic themes and cluster compounds into groups with shared bioactivity profiles. In this context, the compounds **1s**–**30s** were classified into distinct groups according to overlaps in their predicted activities. The resulting clusters reflect convergence around key biological processes, including mitochondrial electron transport, membrane integrity modulation, antiparasitic and antihelmintic activity, and cancer-associated pathways such as TP53 regulation. This systematic grouping provides a rational basis for discussing the pharmacological relevance of the compounds and for prioritizing candidates for further experimental validation.

Group 1 consists of electron transport chain (ETC) modulators characterized by a high probability of ubiquinol–cytochrome-c reductase (Complex III) inhibition, with recurrent overlap in activities such as Aspulvinone dimethylallyltransferase inhibition, cytochrome P450 (CYP) substrate interactions, and testosterone 17β-dehydrogenase inhibition. The representative compounds **1s**–**10s** share a strong mitochondrial and metabolic signature, simultaneously targeting ETC function and steroid metabolism. This dual activity suggests significant potential for metabolic interference, making these molecules promising candidates in anticancer, antimicrobial, and antiparasitic drug discovery.

All of the compounds **1s**–**10s** exhibit the highest inhibitory activity against ubiquinol-cytochrome-c reductase, indicating their suitability as potential inhibitors of this enzyme. Ubiquinol-cytochrome-c reductase inhibitors are compounds that target Complex III of the mitochondrial electron transport chain, also known as the cytochrome bc_1 complex. This enzyme catalyzes the transfer of electrons from ubiquinol (the reduced form of coenzyme Q) to cytochrome c, coupled with proton translocation across the inner mitochondrial membrane. By inhibiting this step, these compounds disrupt the proton gradient and impair ATP synthesis [35].

The high predicted activity of compounds **1s**–**10s** as ubiquinol–cytochrome-c reductase inhibitors can be attributed to their structural capacity to interfere with Complex III of the mitochondrial electron transport chain, a crucial hub for cellular energy production. Inhibitors of this complex are of particular importance because they not only serve as fundamental research tools for dissecting mitochondrial bioenergetics and the Q-cycle mechanism, but also demonstrate significant pharmacological potential. Clinically relevant examples, such as atovaquone, illustrate their value as antiparasitic agents, while strobilurin derivatives highlight their successful application in agriculture as antifungal fungicides. Moreover, Complex III inhibition is closely linked with the induction of oxidative stress, a property that underpins their potential as antimicrobial and anticancer agents, given that many pathogens and tumor cells are highly dependent on mitochondrial function. Finally, by altering electron flow and enhancing reactive oxygen species (ROS) generation, these compounds provide insights into cellular redox balance, mitochondrial signaling, and oxygen-sensing pathways. Thus, the strong activity observed for compounds **1s**–**10s** not only underscores their biological relevance but also positions them as promising scaffolds for future development in therapeutic, agricultural, and mechanistic research contexts [36–38].

Aspulvinone dimethylallyltransferase (EC 2.5.1.35), also known as dimethylallyl pyrophosphate:aspulvinone-E dimethylallyltransferase, is a fungal prenyltransferase that plays a critical role in the biosynthesis of aspulvinone pigments. This enzyme catalyzes the transfer of one or two dimethylallyl moieties from dimethylallyl diphosphate (DMAPP) onto the aromatic compound aspulvinone E, producing mono- and diprenylated derivatives—aspulvinone I and H, respectively. It also accepts aspulvinone G as an alternative substrate. The enzyme is a hexamer composed of ~45 kDa subunits, with optimal activity at pH 7.0 and apparently no requirement for metal cofactors. Notably, the dye bromophenol blue has been found to strongly inhibit its enzymatic activity [39]. Compound **3s**, identified as 3,3′-methylenebis(4-hydroxy-6-methyl-2H-pyran-2-one), exhibited the highest predicted activity, with a probability value approaching 1.000.

The membrane integrity agonist hit exhibited predicted activity values ranging from 0.551 to 0.861, making compound **3s** the most active and **6s** least active, probably due to the existence of the nonpolar and lipophilic residue $-C_6H_{13}$. A membrane integrity agonist is a compound that enhances or preserves the structural and functional stability of cellular membranes. These agents interact with lipid bilayers or membrane-associated proteins to prevent disruptions, maintain barrier properties, and support cellular homeostasis. Maintaining membrane integrity is crucial for protecting cells from environmental stresses, toxins, or pathogens, and is essential for proper cellular signaling and function. Membrane integrity agonists are of interest in various therapeutic contexts, including neuroprotection, anti-inflammatory treatments, and enhancing the efficacy of other bioactive compounds [40].

Group 2 comprises membrane integrity modulators characterized by a consistently predicted membrane-stabilizing (agonist) activity, often accompanied by CDP-glycerol glycerophosphotransferase inhibition, apoptosis induction, and anti-inflammatory and

antioxidant effects. The representative compounds **11s**–**20s**, **23s**, and **24s** integrate membrane-stabilizing properties with cell death–related and immune-modulating activities, suggesting potential dual roles in regulating cell viability and immune responses. This combination of effects indicates their promise for applications in inflammatory diseases, apoptosis-related pathologies, and antimicrobial therapy.

CDP-glycerol glycerophosphotransferase (CGPTase) inhibitors target a key bacterial enzyme responsible for teichoic acid biosynthesis, an essential component of the cell walls in Gram-positive bacteria such as Bacillus subtilis and *Staphylococcus aureus* [41]. CGPTase catalyzes the transfer of glycerol-phosphate units from CDP-glycerol to growing poly(glycerophosphate) chains, a critical step in the formation of wall teichoic acids, which contribute to cell wall integrity, ion homeostasis, and pathogenicity. Inhibition of this enzyme disrupts teichoic acid polymerization, weakening the bacterial cell walls, increasing susceptibility to osmotic stress, and impairing processes such as cell division and biofilm formation [42]. CGPTase inhibitors represent a promising avenue in antimicrobial research, particularly against antibiotic-resistant Gram-positive pathogens, by disrupting a pathway critical for bacterial growth, structural stability, and virulence. This approach highlights the therapeutic potential [43]. Several compounds in this group—specifically **11s**, **12s**, **14s**, **15s**, **17s**, **18s**, and **19s**—have been reported to exhibit antibacterial activity (see Table A2, Biological Activity Assays on Synthetic PGs), with **19s** demonstrating the most pronounced effect.

Group 3 represents an antihelmintic and antiparasitic cluster, characterized by high P_a values for antihelmintic and antiparasitic activity, often accompanied by CDP-glycerol inhibition, apoptosis agonism, and occasionally antineoplastic properties. The representative compounds **20s**–**26s**, **29s**, and **30s** exhibit strong antiparasitic potential alongside overlapping metabolic and membrane-related activities. Notably, the dual antiparasitic–antineoplastic predictions observed in compounds such as **20s**, **22s**, **25s**, and **26s** indicate broad bioactivity profiles, highlighting their potential for application in neglected tropical diseases or as candidates for drug repurposing.

Antihelmintic compounds are critical in combating parasitic worm infections (helminthiasis), which affect over 2 billion people globally, particularly in tropical and subtropical regions [44]. The emergence of drug-resistant strains necessitates the development of new therapeutic agents with novel mechanisms of action [45,46].

Group 4 consists of antineoplastic and TP53-associated modulators, characterized by strong predicted antineoplastic activity, enhancement of TP53 expression, and induction of apoptosis. The representative compounds **26s**–**28s**, with **20s**, **22s**, **25s**, and **30s** as secondary members) are directly linked to tumor suppressor p53 regulation and exhibit broad antineoplastic potential. By modulating TP53, a key hallmark of cancer therapeutics, these compounds are particularly relevant for oncology-focused drug development. The TP53 gene, often called the "guardian of the genome", encodes the tumor suppressor protein p53, which plays a central role in controlling cell cycle progression, DNA repair, apoptosis, and senescence [47]. Under normal conditions, p53 levels are kept low through continuous degradation mediated by the E3 ubiquitin ligase MDM2 [48]. In response to stress signals such as DNA damage, oncogene activation, or hypoxia, p53 is stabilized and activated, leading to the transcription of numerous target genes that determine whether a cell will pause for repair or undergo programmed cell death [49].

Group 5 comprises mixed or pleiotropic modulators, characterized by overlapping immunosuppressant, antieczematic, antifungal, and other metabolic activities, without a single dominant pharmacological cluster. The representative compounds **29s** and **30s**, partially overlapping with Groups 3 and 4, exhibit a polypharmacology profile, affecting multiple pathways including immune regulation, skin-related indications, and metabolic

enzymes. This pleiotropic activity suggests potential as multi-target agents, although further prioritization is needed to define their most relevant therapeutic applications.

Both compounds **29s** and **30s** exhibit testosterone 17 β-dehydrogenase ($NADP^+$) inhibitor activity with P_a values 0.607 and 0.537, respectively. Testosterone 17 β-dehydrogenase ($NADP^+$) inhibitor blocks the activity of the enzyme testosterone 17 β-dehydrogenase that catalyzes the oxidation of testosterone to androst-4-ene-3,17-dione using $NADP^+$ as a cofactor. By inhibiting this enzyme, the conversion between active and inactive forms of steroid hormones, such as testosterone, is reduced, which can impact androgen biosynthesis and regulation of male sex hormones. This enzyme is important in steroid hormone metabolism and targeting its activity may offer therapeutic potential for diseases related to hormone imbalance, including certain cancers and metabolic disorders. The inhibition interferes with the enzyme's role in steroid hormone pathways that influence physiological processes regulated by testosterone [50–52].

Inhibitors of Testosterone 17 β-dehydrogenase ($NADP^+$) can be both beneficial and have potential risks depending on the context. These inhibitors are considered beneficial in treating hormone-dependent diseases such as estrogen receptor-positive breast cancer by reducing active estrogen levels, which slows tumor growth. They may also help manage androgen-related conditions like prostate cancer, benign prostatic hyperplasia, acne, and hirsutism by modulating androgen metabolism. However, since the enzyme plays a crucial role in steroid hormone regulation, inhibition can disturb normal hormonal balance, leading to side effects or compensatory changes in hormone pathways. Due to the enzyme's involvement in critical physiological processes, selective inhibition targeting specific isoforms is important to minimize adverse effects. While promising in preclinical studies, no inhibitors are yet widely clinically used, and further testing is required for safety and efficacy [51,53–55].

Several of the best-characterized biological properties traditionally associated with *Helichrysum* species—specifically antioxidant, anti-inflammatory, antiviral, and antibacterial activities [56,57]—were also reflected in the PASS predictions, thereby supporting the biological relevance of the computational outcomes. The predicted P_a values are presented in Table 1.

Analysis of the antiviral activity predictions indicates that all evaluated compounds are predicted to possess antiviral potential, with varying probabilities of activity.

Among these, several derivatives display particularly pronounced activity. Notable examples include **5s** 6-diethyl-1′-phenyl-6-methylhelipyrone, **13s** 6-diethyl-5,5,6-trimethyl-1′-phenylarzanol, **18s** 1′-phenylarzanol, **9s** 1′-phenylhelipyrone, **4s** 3,3′-(ethane-1,1-diyl)bis(4-hydroxy-6-methyl-2H-pyran-2-one), **2s** helipyrone ketone, **8s** 1′-methylhelipyrone, and **6s** 6-diethyl-1′-hexyl-6-methylhelipyrone. These findings suggest that structural variations within the helipyrone and arzanol scaffolds can significantly influence antiviral potency, highlighting specific substituents as potential determinants of enhanced bioactivity.

Examination of the structures of the four most active compounds reveals a common feature, namely the presence of a phenyl substituent at the 1′-position. This structural element is likely to enhance the hydrophobic character of the molecules, facilitate π–π stacking interactions, and contribute to improved binding affinity at relevant biological targets.

Cycloarzanol A **15s** exhibits the higher potent anti-inflammatory activity, with a P_a range of all compounds between 0.261 and 0.751, positioning it as the most efficacious compound among the arzanol derivatives (Table 1). This finding further supports previous studies demonstrating that arzanol and its analogs possess significant anti-inflammatory properties [16,58].

Table 1. Biological Activities of Phytochemical compounds **1s**–**30s** using PASS program.

Compound	Activities [P_a] *			
	Antioxidant	**Anti-Inflammatory**	**Antiviral**	**Antibacterial**
1s	0.299	0.534	0.257	0.449
2s	0.313	0.509	0.506	0.38
3s	0.281	0.387	0.395	0.438
4s	0.262	0.494	0.592	0.366
5s	0.203	0.359	0.781	0.393
6s	0.274	0.466	0.493	0.321
7s	0.223	0.509	0.293	0.392
8s	0.256	0.493	0.502	0.329
9s	0.196	0.261	0.652	0.359
10s	0.273	0.474	0.442	0.284
11s	0.573	0.702	0.329	0.563
12s	0.633	0.623	0.415	0.510
13s	0.415	0.463	0.715	0.534
14s	0.612	0.602	0.374	0.482
15s	0.631	0.751	0.314	0.460
16s	0.54	0.602	0.351	0.453
17s	0.581	0.579	0.382	0.486
18s	0.362	0.411	0.669	0.510
19s	0.568	0.560	0.348	0.458
20s	0.469	0.713	0.271	0.522
21s	0.541	0.696	0.291	0.541
22s	0.449	0.608	0.265	0.541
23s	0.572	0.637	0.290	0.539
24s	0.486	0.557	0.266	0.539
25s	0.510	0.672	0.259	0.534
26s	0.430	0.592	0.237	0.534
27s	0.421	0.573	0.276	0.453
28s	0.355	0.495	0.254	0.453
29s	0.402	0.635	0.310	0.462
30s	0.305	0.528	0.277	0.461

* The predicted biological activities are expressed as P_a (probability "to be active") estimates the chance that the studied compound is belonging to the sub-class of active compounds (resembles the structures of molecules, which are the most typical in a sub-set of "actives" in PASS training set). The value of the most active compound is 1.

Arzanol, a prenylated heterodimeric phloroglucinyl α-pyrone, has been identified as the primary anti-inflammatory constituent of *Helichrysum italicum*, a Mediterranean medicinal plant traditionally employed in folk medicine for the treatment of inflammatory conditions and infectious diseases [1,59].

It has been extensively studied for its anti-inflammatory effects. It functions through multiple mechanisms, including the inhibition of nuclear factor-kappa B (NF-κB) activation, suppression of pro-inflammatory cytokine release (such as IL-1β, IL-6, IL-8, and TNF-α),

and inhibition of microsomal prostaglandin E2 synthase-1 (mPGES-1) and 5-lipoxygenase (5-LOX) enzymes. These actions collectively contribute to its potent anti-inflammatory activity [8].

Arzanol, also demonstrated antioxidant properties by effectively inhibiting lipid peroxidation in various in vitro systems, and it also protected VERO cells from oxidative stress induced by tert-butyl hydroperoxide (TBH), reducing oxidative damage in these cells without causing cytotoxicity [12]. The observed bioactivity of arzanol derivatives appears to be largely inherited from the parent compound, arzanol, which has been shown to possess notable antioxidant properties (Table 1).

The in silico assessment of the thirty phloroglucinol α-pyrones using PASS online revealed distinct and diverse predicted biological activities, encompassing mitochondrial modulation, membrane stabilization, antiparasitic and antihelmintic effects, antineoplastic potential, and pleiotropic metabolic activities. Compounds **1s–10s** were predicted as strong modulators of the mitochondrial electron transport chain, particularly as ubiquinol–cytochrome-c reductase inhibitors, highlighting their potential in antimicrobial, anticancer, and metabolic interventions. Membrane integrity modulators **11s**–**20s**, **23s**, **24s** and antiparasitic derivatives **20s**–**26s**, **29s**, **30s** demonstrated overlapping bioactivities, suggesting applications in immune regulation, apoptosis, and infectious disease management. Notably, antineoplastic compounds **26s**–**28s** exhibited TP53-associated activity, reinforcing their relevance in oncology. Pleiotropic compounds **29s**, **30s** displayed multi-target potential, including testosterone 17β-dehydrogenase inhibition, indicating additional therapeutic avenues.

The synthetic phloroglucinol α-pyrones investigated in this study exhibited a broad spectrum of predicted biological activities, including anti-inflammatory, antioxidant, antiviral, antibacterial, and metabolic modulatory effects. These in silico predictions are consistent with previously reported experimental findings for arzanol and its analogs, indicating that key pharmacological properties are largely retained across the synthetic derivatives and supporting their potential as promising candidates for further pharmacological and therapeutic exploration.

12. Prediction of Acute Rat Toxicity

To evaluate the potential toxicity of compounds **1s–30s**, we employed the GUSAR software platform. GUSAR was developed to generate quantitative structure–activity and structure–property relationship (QSAR/QSPR) models based on curated training datasets. The software enables in silico prediction of median lethal dose (LD_{50}) values in rats via four routes of administration: oral, intravenous, intraperitoneal, and subcutaneous [60]. The web-based computational platform is extensively employed as predictive tools for assessing toxicological profiles [61–63].

In this study, GUSAR was utilized to perform quantitative in silico toxicity assessment of the *Helichrysum*-derived α-pyrone-phloroglucinols **1s–30s**. The predicted LD_{50} values, expressed in mg/kg, are presented in Figure 3 and summarized in Table A1.

Most compounds fall into OECD Categories 3–4, suggesting moderate to slight acute toxicity. A few compounds exhibit very high LD_{50} values (>2000 mg/kg) via certain routes, indicating practical non-toxicity. Conversely, several compounds show low LD_{50} values (<100 mg/kg) for IV or IP administration, reflecting a higher toxic potential. Compound **28s** 22-methyl-22-ethylitalipyrone triacetate demonstrates the lowest predicted LD_{50} values, particularly via the subcutaneous (12.96 mg/kg) and IP (97.64 mg/kg) routes, placing it in OECD Category 2 (toxic). This indicates that **28s** carries the highest acute toxicity risk among the tested series. Immediately thereafter follows compound **27s**, which differs by the absence of a single methyl group in its structural formula. Compound **6s** 6-diethyl-1′-hexyl-6-methylhelipyrone exhibits very high LD_{50} values across all routes (e.g., SC: 3292.0 mg/kg,

Oral: 775.24 mg/kg) and was explicitly marked as "NonToxic" within the applicability domain of GUSAR. This suggests it is the safest compound in the series, falling within OECD Category 5 (practically non-toxic).

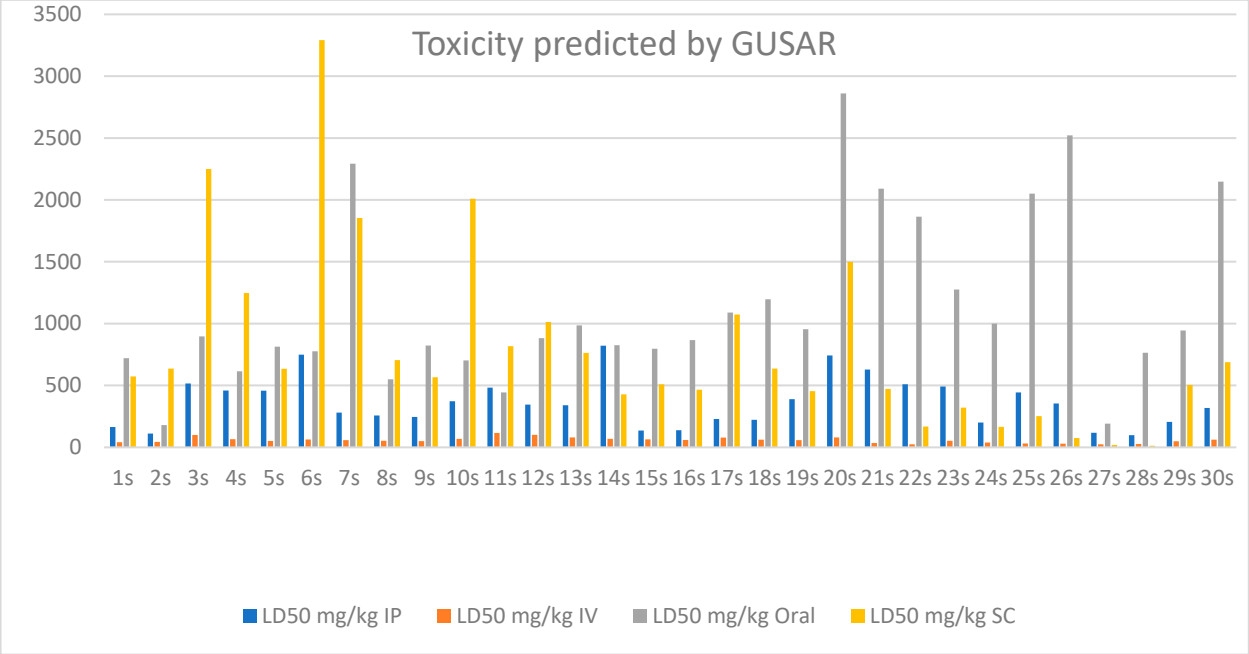

Figure 3. Acute rat toxicity predicted via GUSAR software. IP–intraperitoneal, IV–intravenous, SC–subcutaneous are the routes of administration.

Compounds **1s**–**30s** were grouped based on their predicted OECD acute toxicity classifications. This categorization allowed for the identification of compounds with varying toxicological profiles, ranging from highly toxic to practically non-toxic, thereby facilitating a clear comparison of their relative acute toxicity.

Category 2 compounds, classified as toxic with lethal doses ranging from 5 to 50 mg/kg, include **27s** and **28s**, which are the most hazardous in the series. Specifically, compound **27s** has an estimated subcutaneous (SC) toxicity of 19.36 mg/kg and an intravenous (IV) toxicity of 24.38 mg/kg, while compound **28s** shows greater toxicity with SC and IV values of 12.96 mg/kg and 26.02 mg/kg, respectively.

Category 3 compounds are classified as moderately toxic, with lethal doses ranging from 50 to 300 mg/kg, and include a relatively large group of substances whose toxicity is mainly observed via intravenous (IV) or intraperitoneal (IP) routes. Notable examples are **1s** (IV: 40.64 mg/kg; IP: 163.84 mg/kg), **2s** (IV: 43.33 mg/kg; oral: 179.63 mg/kg), **7s** (IV: 57.48 mg/kg; IP: 280.84 mg/kg), **8s** (IV: 52.59 mg/kg; IP: 256.94 mg/kg), **9s** (IV: 49.24 mg/kg; IP: 245.24 mg/kg), **15s** (IP: 135.64 mg/kg; IV: 64.08 mg/kg), **16s** (IP: 137.74 mg/kg; IV: 59.43 mg/kg), **17s** (IP: 228.14 mg/kg), **18s** (IP: 221.84 mg/kg), **24s** (IV: 38.66 mg/kg; IP: 200.64 mg/kg), and **29s** (IP: 204.64 mg/kg; IV: 48.26 mg/kg).

Category 4 substances are considered slightly toxic, with lethal doses ranging from 300 to 2000 mg/kg, and are generally regarded as safer at moderate exposure levels, though they can still pose some risk. This group includes compounds such as **3s**, which is borderline between Category 3 and 4 with an intravenous (IV) toxicity of 98.76 mg/kg but shows subcutaneous (SC) and oral toxicity values above 800 mg/kg; **4s** (IP: 459.24 mg/kg); **5s** (IP: 458.04 mg/kg); **10s** (IP: 372.14 mg/kg); **11s** (IP: 481.54 mg/kg); **12s** (IP: 345.44 mg/kg); **13s** (IP: 339.14 mg/kg); **14s** (IP: 820.95 mg/kg); **19s** (IP: 388.94 mg/kg); **21s** with IP toxicity of 628.05 mg/kg but a borderline IV value of 34.49 mg/kg; **22s**, which is borderline category

based on IV toxicity at 23.44 mg/kg though other routes show higher values; **23s** (IP: 491.54 mg/kg); **25s** (IP: 442.74 mg/kg); **26s** (IP: 353.74 mg/kg); and **30s** (IP: 317.64 mg/kg).

Category 5 compounds are regarded as practically non-toxic, with lethal doses exceeding 2000 mg/kg, and represent the least hazardous substances within the series. Included in this category are **6s**, which has a subcutaneous (SC) toxicity of 3292.0 mg/kg and an oral toxicity of 775.24 mg/kg, explicitly classified as non-toxic, and **20s**, which shows an oral toxicity of 2860.05 mg/kg.

The in silico assessment of the *Helichrysum*-derived α-pyrone-phloroglucinols **1s**–**30s** revealed a pronounced relationship between structural modifications and predicted acute toxicity. Most compounds were classified within OECD Categories 3 and 4, suggesting moderate to slight toxicity, whereas only a few representatives fell into the extreme categories of toxic (Category 2) or practically non-toxic (Category 5).

The highest acute toxicity was observed for 22-methyl-22-ethylitalipyrone triacetate **28s** and 22,22-dimethylitalipyrone triacetate **27s**, both belonging to the italoipyrone triacetate series. Their low LD_{50} values, particularly via subcutaneous and intravenous routes, can be attributed to the presence of multiple acetyl substituents that reduce polarity and enhance lipophilicity, thereby facilitating rapid systemic absorption [64,65]. Moreover, the triacetate groups act as potential pro-drug functionalities that can be hydrolyzed by esterases [66,67], releasing more reactive or bioactive cores intracellularly, which likely explains their predicted acute toxicity. The small structural difference between **28s** (ethyl + methyl substitution) and **27s** (dimethyl substitution) underscores how subtle steric and electronic variations at the 22-position markedly influence toxicological outcomes.

In contrast, compounds with fewer or no acetyl substituents, such as 6-diethyl-1′-hexyl-6-methylhelipyrone **6s**, exhibited very high LD_{50} values across all routes and were explicitly classified as non-toxic, falling into OECD Category 5. Its non-acetylated structure and long alkyl chain contribute to higher metabolic stability and reduced systemic toxicity, positioning **6s** as the safest compound in the series. Similarly, arzanol derivatives and simple pyrone scaffolds (e.g., **1s**–**5s**, **10s**–**19s**) tended to show intermediate toxicity (Categories 3–4), where the balance between lipophilic substituents (e.g., hexyl, phenyl) and polar hydroxyl groups dictated their absorption and toxic potential.

Taken together, the results highlight a clear structure–toxicity relationship within this compound class: acetylation and bulky alkyl substitutions significantly enhance acute toxicity, whereas non-acetylated analogs and balanced polarity confer relative safety. These findings provide useful guidance for prioritizing derivatives in further pharmacological or toxicological investigations. Of course these structure–toxicity relationships should be interpreted cautiously, as GUSAR predictions do not account for metabolism or chronic exposure.

13. Lipophilicity

Lipophilicity is one of the most important physicochemical parameters in medicinal chemistry, as it strongly influences the pharmacokinetic and pharmacodynamic properties of bioactive molecules. It describes the affinity of a compound for lipophilic versus aqueous environments and is commonly expressed as the octanol/water partition coefficient (logP) or, for ionizable compounds, the distribution coefficient (logD). Lipophilicity affects membrane permeability, aqueous solubility, plasma protein binding, tissue distribution, metabolic stability, and ultimately the absorption, distribution, metabolism, excretion, and toxicity (ADMET) profile of drug candidates. Moreover, it plays a crucial role in ligand–target recognition, since hydrophobic interactions frequently contribute to the stability of protein–ligand complexes. Consequently, optimization of lipophilicity is considered a fundamental aspect of drug design, where an appropriate balance between hydrophobicity

and hydrophilicity is required to maximize biological activity while maintaining favorable pharmacokinetic properties. Excessive lipophilicity often leads to poor aqueous solubility, increased metabolic clearance, and higher nonspecific binding, whereas insufficient lipophilicity may limit membrane permeability and target affinity [68–70].

The calculated octanol/water partition coefficients cLogP of the discussed compounds were estimated using ChemBioDraw Ultra, Version 20.0 (PerkinElmer Informatics Inc., Waltham, MA, USA). The software utilizes validated fragment-based algorithms to predict lipophilicity. Due to its robust predictive performance and extensive use in medicinal chemistry research, ChemBioDraw is widely recognized as a reliable computational tool for the estimation of molecular lipophilicity [71,72].

Lipophilicity is one of the key molecular descriptors influencing the pharmacokinetic behavior of biologically active compounds, affecting membrane permeability, aqueous solubility, plasma protein binding, tissue distribution, and ultimately biological efficacy. The calculated partition coefficient (cLogP) was therefore determined for all compounds **1s–30s** to evaluate the influence of the structural modifications introduced throughout the different classes of α-pyrone derivatives (Table 2). The calculated cLogP values ranged from 1.89 **3s** to 6.77 **19s**, indicating a broad physicochemical diversity within the studied series. The observed differences closely follow the structural evolution from simple α-pyrone derivatives to more complex phloroglucinol–α–pyrone hybrids and their protected analogues. The simplest monopyrone derivatives **1s** (cLogP = 1.96), **2s** (2.19), **3s** (1.89) and **4s** (1.99) exhibit the lowest lipophilicity because their structures contain only a single α-pyrone scaffold with a limited number of hydrophobic carbon atoms and several oxygen-containing functional groups capable of increasing polarity. The slight increase observed for **2s** compared with **1s** can be attributed to the additional ketone-containing alkyl side chain, which increases molecular size despite introducing another carbonyl group.

Table 2. Calculated octanol/water partition coefficients (cLogP) of the discussed compounds.

Compound	cLogP	Compound	cLogP
1s	1.9593	**16s**	4.7541
2s	2.1853	**17s**	4.1257
3s	1.8876	**18s**	5.1647
4s	1.9866	**19s**	6.7707
5s	3.0256	**20s**	3.4061
6s	4.6316	**21s**	4.2441
7s	2.7380	**22s**	4.7731
8s	3.8426	**23s**	6.0283
9s	4.8816	**24s**	6.5573
10s	6.4876	**25s**	4.8141
11s	3.5487	**26s**	5.3431
12s	3.1977	**27s**	4.1111
13s	4.2367	**28s**	4.6401
14s	5.8427	**29s**	3.5746
15s	4.8041	**30s**	4.1036

A pronounced increase in lipophilicity is observed after aldehyde-mediated dimerization of the α-pyrone nucleus. Formation of symmetrical dipyrone derivatives substantially enlarges the hydrophobic molecular surface by introducing a second pyrone ring connected through a methylene bridge. Furthermore, the nature of the substituent attached to the bridging carbon strongly affects cLogP. Replacement of hydrogen or methyl substituents with phenyl **5s**, cLogP = 3.03 and especially hexyl groups **6s**, cLogP = 4.63 produces a marked increase in lipophilicity. The same tendency is even more evident in compounds **8s–10s**, where the additional ethyl substituent already present on the pyrone ring further

increases hydrophobicity, resulting in cLogP values of 3.84, 4.88, and 6.49, respectively. This demonstrates that elongation of aliphatic chains contributes more significantly to lipophilicity than aromatic substitution alone (Table 2).

The arzanol derivatives **11s–19s** display intermediate to high lipophilicity cLogP = 3.20–6.77, reflecting the balance between the highly oxygenated phloroglucinol fragment and the increasingly hydrophobic substituents introduced during analogue synthesis. Although incorporation of the phloroglucinol moiety introduces three phenolic hydroxyl groups capable of hydrogen bonding, these polar functionalities are counterbalanced by the larger aromatic framework and lipophilic side chains. Again, substitution with phenyl **13s**, **18s** and particularly hexyl **14s**, **19s** groups produces the largest increase in cLogP, with **19s** exhibiting the highest lipophilicity of the entire series cLogP = 6.77. Interestingly, these two compounds were also reported as the most potent dual mPGES-1/5-LO inhibitors, suggesting that increased hydrophobicity may enhance interactions with the predominantly hydrophobic regions of the enzyme binding sites. Nevertheless, this relationship should be interpreted cautiously, since biological activity is also governed by molecular geometry, hydrogen-bonding capability, and electronic effects rather than lipophilicity alone.

Cyclization of arzanol to give cycloarzanol A **15s** and cycloarzanol B **16s** produces only a minor decrease in cLogP (4.80 and 4.75, respectively) compared with the corresponding open-chain analogues. Because cyclization does not significantly alter the elemental composition but mainly increases molecular rigidity, only small changes in calculated lipophilicity are expected. Thus, cyclization primarily affects molecular conformation rather than overall hydrophobic character.

The most lipophilic compounds among the protected derivatives are the methyl ethers **23s** cLogP = 6.03 and **24s** (6.56). Methylation converts phenolic hydroxyl groups into methoxy substituents, eliminating hydrogen-bond donor capacity while increasing the hydrophobic surface area. A similar trend is observed for the acetylated derivatives (**20s**–**22s**, **25s**–**30s**), where acetyl protection masks phenolic hydroxyl groups and decreases molecular polarity. Consequently, these derivatives generally possess cLogP values between 3.4 and 5.3, reflecting improved lipophilicity compared with the corresponding non-protected analogues.

Overall, the calculated lipophilicity follows the expected structure–property relationship throughout the series. Increasing molecular size, incorporation of additional aromatic rings, extension of aliphatic side chains, and masking of phenolic hydroxyl groups through methylation or acetylation all contribute to higher cLogP values. Conversely, the presence of free hydroxyl groups and relatively small α-pyrone frameworks maintain lower lipophilicity. Most compounds exhibit cLogP values between 3 and 5, a range generally considered favorable for passive membrane permeation while still maintaining acceptable drug-like properties. Only compounds **10s**, **19s**, **23s**, and **24s** exceed a cLogP value of 6, suggesting that although these derivatives may possess enhanced membrane affinity, they may also exhibit reduced aqueous solubility and increased plasma protein binding. Therefore, optimization of lipophilicity should be considered alongside biological activity during the future development of α-pyrone–phloroglucinol derivatives.

14. Conclusions

This review presents the synthesis and biological evaluation of several natural and synthetic phloroglucinol-based α-pyrone derivatives, encompassing monopyrones, dipyrones, arzanol analogues, and their functionalized derivatives. The synthetic approaches demonstrate versatility, from simple β-keto ester cyclodehydration yielding monopyrones (74% yield) to sophisticated carba-Betti-type multicomponent condensations producing arzanol and analogues (30–68% yields). Key transformations include aldehyde-mediated

homodimerization for symmetrical dipyrones, TBAF-catalyzed heterodimerization for arzanol synthesis using either paraformaldehyde or Eschenmoser's salt as methylene donors, and acid-catalyzed intramolecular cyclization generating cycloarzanol A and B. Post-synthetic modifications through acetylation and methylation provided access to less polar derivatives with quantitative yields in most cases. The modular nature of these synthetic strategies, particularly the flexibility in aldehyde selection and pyrone substitution patterns, enables systematic exploration of structural diversity. This compilation provides a structured foundation for future synthetic efforts, highlighting the accessibility of these natural product-inspired scaffolds through straightforward, scalable chemistry that bridges synthetic methodology with natural product biosynthesis.

The proposed retrosynthetic approaches further extend the synthetic landscape of *Helichrysum*-derived α-pyrones by outlining unified and modular strategies toward structurally complex heterodimeric natural products and their analogues.

The in silico analysis using PASS and GUSAR revealed that the phloroglucinol-based α-pyrone derivatives possess diverse and relevant predicted biological activities, including anti-inflammatory, antimicrobial, antiparasitic, and antineoplastic effects. The predicted activity profiles were consistent with reported experimental data for arzanol and related compounds, supporting the validity of the computational approach. Toxicity predictions indicated generally acceptable safety profiles, with clear structure–toxicity relationships. The calculated lipophilicity (cLogP) values further complemented the structural and biological analysis, demonstrating that modifications of the α-pyrone and phloroglucinol scaffolds substantially influence the physicochemical properties of these derivatives.

Author Contributions: Conceptualization, Y.V.; methodology, S.M. and I.I.; data curation, K.K.; writing—original draft preparation, Y.V.; writing—review and editing, S.M. and I.I. All authors have read and agreed to the published version of the manuscript.

Funding: This research received no external funding.

Institutional Review Board Statement: Not applicable.

Informed Consent Statement: Not applicable.

Data Availability Statement: The data presented in this study are available in this article.

Acknowledgments: The research was supported by the Council of Medical Sciences, Medical University of Sofia, Bulgaria. Grant number: 141/29.05.2024.

Conflicts of Interest: The authors declare no conflicts of interest.

Appendix A

Table A1. Synthetic conditions.

Compound Name	Exact Mass (Da), Elem. Comp.	Starting Compounds	Synthesis Conditions	Isolated (mg), Yield (%)	Reference
helipyrone	320.1260 ($C_{17}H_{20}O_6$)	6-Ethyl-4-hydroxy-5-methyl-α-pyrone (**1i**); formaldehyde	1i (200 mg, 1.30 mmol) in $CHCl_3$ (3 mL) was treated with paraformaldehyde (19.5 mg, 0.65 mmol) and stirred 16 h/40 °C. Solvent removed; residue purified by silica GCC (petroleum ether/EtOAc 7:3).	142 mg (68%)	[2]
arzanol	402.1678 ($C_{22}H_{26}O_7$)	6-Ethyl-4-hydroxy-5-methyl-α-pyrone (**1i**), paraformaldehyde, phloracetophenone (**2i**), TBAF	(Procedure A) 1i (17 mg, 0.11 mmol), paraformaldehyde (3 mg, 0.11 mmol), 2i (50 mg, 0.11 mmol), TBAF (1 M in THF, 220 µL, 0.22 mmol) in $CHCl_3$ (1.5 mL), stir 16 h at 40 °C; quench with 2 N H_2SO_4, extract with CH_2Cl_2, dry, silica gel GCC (PE + AcOH)	27 mg (61%)	[2]

Table A1. *Cont.*

Compound Name	Exact Mass (Da), Elem. Comp.	Starting Compounds	Synthesis Conditions	Isolated (mg), Yield (%)	Reference
		6-Ethyl-4-hydroxy-5-methyl-α-pyrone (**1i**), Eschenmoser's salt, phloracetophenone (**2i**), TBAF	(Procedure B) 1i (17 mg, 0.11 mmol), Eschenmoser's salt (15 mg, 0.11 mmol), 2i (50 mg, 0.11 mmol), TBAF (1 M in THF, 220 µL, 0.22 mmol) in $CHCl_3$ (1.5 mL), stir 16 h at 40 °C; quench with 2 N H_2SO_4, extract with CH_2Cl_2, dry, silica gel GCC (PE + AcOH)	29 mg (65%)	[2]
6-ethyl-4-hydroxy-5-methyl-α-pyrone (1s)	154.0630 ($C_8H_{10}O_3$)	ethyl 3-oxopentanoate (**3i**); ethyl propionate; NaH; *n*-BuLi; polyphosphoric acid	Step 1: NaH (60%, 195 mg, 3.9 mmol) in dry THF (15 mL, 0 °C) was treated with ethyl 3i (500 µL, 3.9 mmol). After 10 min n-BuLi (2.5 M, 1.56 mL, 3.9 mmol) was added, followed by ethyl propionate (223 µL, 1.95 mmol). A second n-BuLi portion (937 µL, 2.34 mmol) and ethyl propionate (223 µL, 1.95 mmol) were introduced 15 min apart. After 15 min the mixture was quenched (conc. HCl), extracted with Et_2O, washed (sat. $NaHCO_3$), dried (Na_2SO_4) and purified by silica gravity column chromatography (petroleum ether/EtOAc 9:1) to give ethyl 4-methyl-3,5-dioxoheptanoate (483 mg, 62%). Step 2: ethyl 4-methyl-3,5-dioxoheptanoate (483 mg, 2.4 mmol) stirred in polyphosphoric acid (1.5 g, 120 °C, 1.5 h), poured on ice, filtered and washed with H_2O to yield the product 6-Ethyl-4-hydroxy-5-methyl-α-pyrone **1s**.	274 mg (74%)	[2]
helipyrone ketone (2s)	238.1205 ($C_{13}H_{18}O_4$)	helipyrone (**20**)	helipyrone (100 mg, 0.36 mmol) was refluxed 20 min in 2% aqueous Na_2CO_3 (50 mL). After cooling, the mixture was acidified (pH ~2), extracted with $CHCl_3$ and the extract purified by silica-gel chromatography (toluene/acetone 9:1) to yield ketone **2s**.	60 mg (60%)	[6]
3,3′-methylenebis(4-hydroxy-6-methyl-2H-pyran-2-one) (3s)	264.0634 ($C_{13}H_{12}O_6$)	6-methyl-4-hydroxypyrone; formaldehyde	As for helipyrone (**6**)	63%	[2]
3,3′-(ethane-1,1-diyl)bis(4-hydroxy-6-methyl-2H-pyran-2-one) (4s)	278.0790 ($C_{14}H_{14}O_6$)	6-methyl-4-hydroxypyrone; isobutyraldehyde	As for helipyrone (**6**)	60%	[2]
6-diethyl-1′-phenyl-6-methyl-helipyrone (5s)	340.0947 ($C_{19}H_{16}O_6$)	6-methyl-4-hydroxypyrone; benzaldehyde	As for helipyrone (**6**)	55%	[2]
6-diethyl-1′-hexyl-6-methyl-helipyrone (6s)	348.1573 ($C_{19}H_{24}O_6$)	6-methyl-4-hydroxypyrone; hexanal	As for helipyrone (**6**)	68%	[2]
helipyrone diacetate (7s)	404.1471 ($C_{21}H_{24}O_8$)	helipyrone (**6**)	helipyrone (**6**) was acetylated with acetic anhydride under standard pyridine conditions	NR	[19]
1′-methyl-helipyrone (8s)	334.1416 ($C_{18}H_{22}O_6$)	6-ethyl-4-hydroxy-5-methyl-α-pyrone (**1i**); acetaldehyde	As for helipyrone (**6**)	65%	[2]
1′-phenyl-helipyrone (9s)	396.1573 ($C_{23}H_{24}O_6$)	6-ethyl-4-hydroxy-5-methyl-α-pyrone (**1i**); benzaldehyde	As for helipyrone (**6**)	52%	[2]
1′-hexylhelipyrone (10s)	404.2199 ($C_{23}H_{32}O_6$)	6-ethyl-4-hydroxy-5-methyl-α-pyrone (**1i**); hexanal	As for helipyrone (**6**)	66%	[2]

Table A1. *Cont.*

Compound Name	Exact Mass (Da), Elem. Comp.	Starting Compounds	Synthesis Conditions	Isolated (mg), Yield (%)	Reference
6-diethyl-5,5,6-trimethylarzanol (11s)	374.1365 ($C_{20}H_{22}O_7$)	6-methyl-4-hydroxypyrone; phloracetophenone (**2i**); paraformaldehyde	6-methyl-4-hydroxypyrone (0.11 mmol), paraformaldehyde (0.11 mmol) and phloracetophenone (2i) (0.11 mmol) in $CHCl_3$ (1.5 mL) were treated with TBAF (1 M, 220 µL, 0.22 mmol) and stirred 16 h/40 °C; quench with 2 N H_2SO_4, extract with CH_2Cl_2, dry, silica gel GCC (PE + AcOH).	58%	[2]
6-diethyl-1′,5,5,6-tetramethylarzanol (12s)	388.1522 ($C_{21}H_{24}O_7$)	6-ethyl-4-hydroxy-5-methyl-α-pyrone (**1**); phloracetophenone (**2i**); isobutyraldehyde	As for **11s**	55%	[2]
6-diethyl-5,5,6-trimethyl-1′-phenylarzanol (13s)	450.1678 ($C_{26}H_{26}O_7$)	triacetic acid lactone (6-methyl-4-hydroxypyrone); phloracetophenone (**2i**); benzaldehyde-iminium	As for **11s**	30 mg (30%)	[2]
6-diethyl-1′-hexyl-5,5,6-trimethylarzanol (14s)	458.2304 ($C_{26}H_{34}O_7$)	6-methyl-4-hydroxypyrone; phloracetophenone (**2i**); hexanal	As for **11s**	40%	[2]
cycloarzanol A (15s)	402.1678 ($C_{22}H_{26}O_7$)	arzanol (**10**)	$CeCl_3$ method: arzanol (100 mg, 0.25 mmol) in dry THF (1 mL) plus $CeCl_3 \cdot 7H_2O$ (100 mg); stir at room temperature 1 week. Work up with EtOAc, sat. $NaHCO_3$, brine; purify by silica gel column (petroleum ether/EtOAc 95:5).	28 mg (28%)	[1]
cycloarzanol A (15s)	402.1678 ($C_{22}H_{26}O_7$)	arzanol (**10**)	HCl method: arzanol (100 mg, 0.25 mmol) in MeOH (5 mL) with HCl (from 100 µL $SOCl_2$), stir at 0 °C 1 h, then room temperature overnight. Work up with EtOAc, sat. $NaHCO_3$, brine; purify by silica gel column (petroleum ether/EtOAc 95:5).	29 mg (29%)	[1]
cycloarzanol B (16s)	402.1678 ($C_{22}H_{26}O_7$)	arzanol (**10**)	$CeCl_3$ method: arzanol (100 mg, 0.25 mmol) in dry THF (1 mL) plus $CeCl_3 \cdot 7H_2O$ (100 mg); stir at room temperature 1 week. Work up with EtOAc, sat. $NaHCO_3$, brine; purify by silica gel column (petroleum ether/EtOAc 95:5).	18 mg (18%)	[1]
cycloarzanol B (16s)	402.1678 ($C_{22}H_{26}O_7$)	arzanol (**10**)	HCl method: arzanol (100 mg, 0.25 mmol) in MeOH (5 mL) with HCl (from 100 µL $SOCl_2$), stir at 0 °C 1 h, then room temperature overnight. Work up with EtOAc, sat. $NaHCO_3$, brine; purify by silica gel column (petroleum ether/EtOAc 95:5).	6 mg (6%)	[1]
1′-methylarzanol (17s)	416.1835 ($C_{23}H_{28}O_7$)	6-ethyl-4-hydroxy-5-methyl-α-pyrone (**1i**); phloracetophenone (**2i**); acetaldehyde	As for the synthesis of arzanol (**10**), Procedure A	68%	[2]
1′-phenylarzanol (18s)	478.1991 ($C_{28}H_{30}O_7$)	6-ethyl-4-hydroxy-5-methyl-α-pyrone (**1i**); phloracetophenone (**2i**); benzaldehyde-iminium (Eschenmoser salt)	As for the synthesis of arzanol (**10**), Procedure B	31 mg (31%)	[2]
1′-hexylarzanol (19s)	486.2617 ($C_{28}H_{38}O_7$)	6-ethyl-4-hydroxy-5-methyl-α-pyrone (**1i**); phloracetophenone (**2i**); hexanal	As for the synthesis of arzanol (**10**), Procedure A	48%	[2]

Table A1. *Cont.*

Compound Name	Exact Mass (Da), Elem. Comp.	Starting Compounds	Synthesis Conditions	Isolated (mg), Yield (%)	Reference
arzanol tetra-acetate (20s)	570.2101 ($C_{30}H_{34}O_{11}$)	arzanol (**1a**)	To a solution of arzanol (200 mg, 0.50 mmol) in dry pyridine (2 mL) was added excess Ac_2O (2 mL). Stir overnight rt; quench with MeOH, dilute with H_2O, extract with Et_2O, sequentially wash (2 N H_2SO_4/$NaHCO_3$/brine), evaporate and wash residue with Et_2O to give product.	198 mg (70%)	[1]
6-*O*-desmethyl-auricepyrone tetraacetate (21s)	598.2414 ($C_{32}H_{38}O_{11}$)	6-*O*-desmethylauricepyrone (**13**)	A stirred solution of 13 (24 mg, 0.05 mmol) in anhydrous $CHCl_3$ (1 mL) was treated with 4-pyrrolidinopyridine (20 mg, 0.16 mmol) and Ac_2O (0.10 mL, 1.06 mmol). The mixture was refluxed for 3 h under N_2, concentrated in vacuo and the residue purified by silica-gel chromatography (petroleum ether/Et_2O 1:1) to give **21s**.	≈20 mg (of a 25 mg of compound **3** + compound **4** mixture), ≈83% (combined)	[6]
23-methyl-6-*O*-desmethylauricepyrone tetraacetate (22s)	612.2571 ($C_{33}H_{40}O_{11}$)	23-methyl-6-*O*-desmethylauricepyrone (**16**)	As described for compound **21s** (same reagent ratios and work-up); product co-eluted with **21s** and was not further separated.	≈5 mg (of a 25 mg of compound **3** + compound **4** mixture), ≈83% (combined)	[6]
auricepyrone dimethyl ether (23s)	458.2304 ($C_{26}H_{34}O_7$)	auricepyrone (**19**)	To a solution of the natural-product mixture of auricepyrone (**19**) (20 mg, ca 1:1 *w*/*w*) in dry diethyl ether (2 mL) was added an ethereal solution of diazomethane until the yellow colour persisted; the reaction stood 1 h at room temperature. Solvent was removed in vacuo and the residue purified by silica gel chromatography (ether: petroleum ether 1:1) to give the colourless oil of **23s** and **24s**.	20 mg (quantitative)	[18]
23-methylauricepyrone dimethyl ether (24s)	472.2461 ($C_{27}H_{36}O_7$)	23-methylauricepyrone (**20**)	As for **23s**	20 mg (quantitative)	[18]
auricepyrone triacetate (25s)	570.2465 ($C_{31}H_{38}O_{10}$)	auricepyrone (**19**)	To a boiling solution of compound 19 (10 mg) in $CHCl_3$ (1 mL) were added 4-pyrrolidinopyridine (20 mg) and acetic anhydride (0.10 mL). After 3 h under reflux the mixture was concentrated and chromatographed on silica (ether: petroleum ether 3:1) to yield the inseparable triacetates auricepyrone triacetate **25s** as colourless oil.	10 mg (quantitative)	[18]
23-methylauricepyrone triacetate (26s)	584.2621 ($C_{32}H_{40}O_{10}$)	23-methylauricepyrone (**20**)	As for **25s**	10 mg (quantitative)	[18]
22,22-dimethylitalipyrone triacetate (27s)	554.2152 ($C_{30}H_{34}O_{10}$)	22,22-dimethylitalipyrone	A suspension of 22,22-dimethylitalipyrone in $CHCl_3$ was refluxed for 2 h with Ac_2O and catalytic 4-pyrrolidinopyridine under N_2. Solvent removal followed by silica-gel chromatography (cyclohexane/EtOAc 9:1).	NR	[6]
22-methyl-22-ethylitalipyrone triacetate (28s)	568.2308 ($C_{31}H_{36}O_{10}$)	22-methyl-22-ethylitalipyrone	As for **27s**	NR	[6]
italidipyrone tetraacetate (29s)	738.2524 ($C_{38}H_{42}O_{15}$)	italidipyrone (**43**)	A solution of italidipyrone (50 mg, 0.09 mmol) in pyridine (3 mL) was treated with Ac_2O (2 mL, 21 mmol) and allowed to stand 24 h at 20 °C. After quenching with ice-water, the mixture was extracted with $CHCl_3$ and the organic layer evaporated; crystallisation from $CHCl_3$/Et_2O afforded tetraacetate **29s**.	25 mg (72%)	[6]

Table A1. *Cont.*

Compound Name	Exact Mass (Da), Elem. Comp.	Starting Compounds	Synthesis Conditions	Isolated (mg), Yield (%)	Reference
23-methylitalidi-pyrone tetraacetate (30s)	752.2680 ($C_{39}H_{44}O_{15}$)	23-methylitalidipyrone (**44**)	As for **29s**	11 mg (72%)	[6]

Table A2. Biological activity assays on synthetic PGs.

Compound Name	Biological Activity	Reference
3,3′-methylenebis(4-hydroxy-6-methyl-2H-pyran-2-one) (3s)	Inactive: mPGES-1 IC_{50} > 100 μM; 5-LO not determined.	[2]
3,3′-(ethane-1,1-diyl)bis(4-hydroxy-6-methyl-2H-pyran-2-one) (4s)	Weak inhibitor: against mPGES-1 (IC_{50} 99 μM) and against 5-LO (IC_{50} 88 μM).	[2]
6-diethyl-1′-phenyl-6-methylhelipyrone (5s)	Weak inhibitor: against mPGES-1 (IC_{50} 93 μM); against 5-LO (IC_{50} 82 μM).	[2]
6-diethyl-1′-hexyl-6-methylhelipyrone (6s)	Weak dual inhibitor: against mPGES-1 (IC_{50} 79 μM) and against 5-LO (IC_{50} 7.8 μM); ~10-fold preference for 5-LO.	[2]
1′-methylhelipyrone (8s)	Inactive: mPGES-1 IC_{50} > 100 μM; 5-LO retains 83% activity at 10 μM, indicating very weak inhibition.	[2]
1′-phenylhelipyrone (9s)	Weak inhibitor: against mPGES-1 (IC_{50} 67 μM) and against 5-LO (IC_{50} 86 μM).	[2]
1′-hexylhelipyrone (10s)	Moderate dual inhibitor: against mPGES-1 (IC_{50} 0.84 μM) and against 5-LO (IC_{50} 56 μM); ~67-fold preference for mPGES-1.	[2]
6-diethyl-5,5,6-trimethylarzanol (11s)	Moderate dual inhibitor: low-micromolar potency on mPGES-1 (IC_{50} 1.0 μM) and mid-micromolar on 5-LO (IC_{50} 9.5 μM); ~10-fold selectivity towards mPGES-1.	[2]
	Potent antibacterial activity in the microdilution assay against six MDR S. aureus strains: SA1199B MIC 1 $\mu g/mL^{-1}$; ATCC 25923 MIC 1 $\mu g/mL^{-1}$; RN4220 MIC 2 $\mu g/mL^{-1}$; EMRSA-15 MIC 2 $\mu g/mL^{-1}$; EMRSA-16 MIC 2 $\mu g/mL^{-1}$; XU212 MIC 16 $\mu g/mL^{-1}$.	[3]
6-diethyl-1′,5,5,6-tetramethylarzanol (12s)	Dual inhibitor: against mPGES-1 (IC_{50} 2.4 μM); against 5-LO activity (IC_{50} 7.9 μM); ~3-fold preference for mPGES-1.	[2]
	Poor antibacterial activity observed by broth-microdilution against MDR *S. aureus* strains: ATCC 25923 MIC 64 $\mu g/mL^{-1}$; SA1199B, RN4220, EMRSA-15, EMRSA-16 MIC 128 $\mu g/mL^{-1}$; XU212 MIC > 128 $\mu g/mL^{-1}$.	[3]
6-diethyl-5,5,6-trimethyl-1′-phenylarzanol (13s)	Dual inhibitor: against mPGES-1 (IC_{50} 1.1 μM); against 5-LO inhibition (IC_{50} 8.4 μM); ~8-fold selectivity for mPGES-1.	[2]
6-diethyl-1′-hexyl-5,5,6-trimethylarzanol (14s)	Potent dual inhibitor: against mPGES-1 inhibition (IC_{50} 0.2 μM); against 5-LO (IC_{50} 1.2 μM); ~6-fold selectivity for mPGES-1.	[2]

Table A2. *Cont.*

Compound Name	Biological Activity	Reference
	Moderate antibacterial activity in the broth-microdilution assay against six MDR S. aureus strains: SA1199B MIC 16 μg/mL^{-1}; XU212 MIC 16 μg/mL^{-1}; ATCC 25923 MIC 8 μg/mL^{-1}; RN4220 MIC 8 μg/mL^{-1}; EMRSA-15 MIC 16 μg/mL^{-1}; EMRSA-16 MIC 8 μg/mL^{-1}.	[3]
cycloarzanol A (15s)	Low antibacterial potency against multidrug-resistant (MDR) *Staphylococcus aureus* isolates in broth-microdilution: ATCC 25923 MIC 32 μg/mL^{-1}; RN4220 MIC 32 μg/mL^{-1}; SA1199B, XU212, EMRSA-15 MIC 128 μg/mL^{-1}; EMRSA-16 MIC > 128 μg/mL^{-1}.	[3]
cycloarzanol B (16s)	Inactive against MDR *Staphylococcus aureus* isolates in the antibacterial broth-microdilution assay: (SA1199B, XU212, ATCC 25923, RN4220, EMRSA-15, EMRSA-16) showed MIC > 128 μg/mL^{-1}.	[3]
1′-methylarzanol (17s)	Dual inhibitor: against mPGES-1 with IC_{50} 2.1 μM; against 5-LO with IC_{50} 5.9 μM; ~3-fold mPGES-1 preference.	[2]
	Weak-to-moderate antibacterial activity against MDR *Staphylococcus aureus* isolates (broth-microdilution, Mueller-Hinton): SA1199B MIC 32 μg/mL^{-1}; RN4220 MIC 32 μg/mL^{-1}; EMRSA-15 MIC 32 μg/mL^{-1}; XU212, ATCC 25923, EMRSA-16 MIC 128 μg/mL^{-1}.	[3]
1′-phenylarzanol (18s)	Dual inhibitor: against mPGES-1 (IC_{50} 0.8 μM); against 5-LO inhibition (IC_{50} 4.9 μM); ~6-fold preference for mPGES-1.	[2]
	Moderate antibacterial activity determined by broth-microdilution against six *S. aureus* MDR strains: SA1199B MIC 16 μg/mL^{-1}; XU212 MIC 4 μg/mL^{-1}; ATCC 25923 MIC 8 μg/mL^{-1}; RN4220 MIC 2 μg/mL^{-1}; EMRSA-15 MIC 6 μg/mL^{-1}; EMRSA-16 MIC 8 μg/mL^{-1}.	[3]
1′-hexylarzanol (19s)	Potent dual inhibitor: against mPGES-1 (IC_{50} 0.3 μM); against 5-LO (IC_{50} 1.6 μM); ~5-fold preference for mPGES-1.	[2]
	Good antibacterial activity in the broth-microdilution assay versus six *S. aureus* MDR strains: SA1199B MIC 4 μg/mL^{-1}; XU212 MIC 8 μg/mL^{-1}; ATCC 25923 MIC 4 μg/mL^{-1}; RN4220 MIC 4 μg/mL^{-1}; EMRSA-15 MIC 8 μg/mL^{-1}; EMRSA-16 MIC 8 μg/mL^{-1}.	[3]

Table A3. Molecular characteristics of synthetic PGs.

Compound Name	Structural Formula	Exact Mass (Da), Elem. Comp.	Class	SMILES	Reference
6-ethyl-4-hydroxy-5-methyl-α-pyrone (1s)	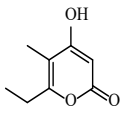	154.063 ($C_8H_{10}O_3$)	monopyrone	O=C(O1)C=C(O)C(C)=C1CC	[2]
eelipyrone ketone (2s)	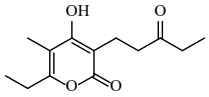	238.1205 ($C_{13}H_{18}O_4$)	monopyrone	OC(C(C)=C(OC1=O)CC)=C1CCC(CC)=O	[6]
3,3′-methylenebis(4-hydroxy-6-methyl-2H-pyran-2-one) (3s)	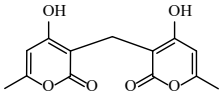	264.0634 ($C_{13}H_{12}O_6$)	dipyrones	CC1=CC(O)=C(CC2=C(O)C=C(C)OC2=O)C(O1)=O	[2]
3,3′-(ethane-1,1-diyl)bis(4-hydroxy-6-methyl-2H-pyran-2-one) (4s)	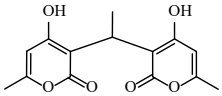	278.079 ($C_{14}H_{14}O_6$)	dipyrones	CC1=CC(O)=C(C(C)C2=C(O)C=C(C)OC2=O)C(O1)=O	[2]
6-diethyl-1′-phenyl-6-methylhelipyrone (5s)	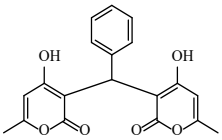	340.0947 ($C_{19}H_{16}O_6$)	dipyrones	CC1=CC(O)=C(C(C2=CC=CC=C2)C3=C(O)C=C(C)OC3=O)C(O1)=O	[2]
6-diethyl-1′-hexyl-6-methylhelipyrone (6s)	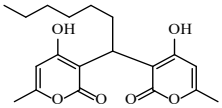	348.1573 ($C_{19}H_{24}O_6$)	dipyrones	CC1=CC(O)=C(C(CCCCCC)C2=C(O)C=C(C)OC2=O)C(O1)=O	[2]
helipyrone diacetate (7s)	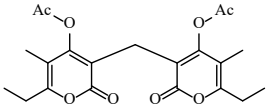	404.1471 ($C_{21}H_{24}O_8$)	dipyrones	CCC1=C(C)C(OC(C)=O)=C(CC2=C(OC(C)=O)C(C)=C(CC)OC2=O)C(O1)=O	[19]
1′-methylhelipyrone (8s)	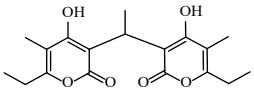	334.1416 ($C_{18}H_{22}O_6$)	dipyrones	CCC1=C(C)C(O)=C(C(C)C2=C(O)C(C)=C(CC)OC2=O)C(O1)=O	[2]
1′-phenylhelipyrone (9s)	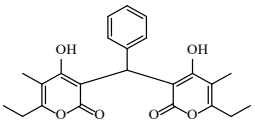	396.1573 ($C_{23}H_{24}O_6$)	dipyrones	CCC1=C(C)C(O)=C(C(C2=CC=CC=C2)C3=C(O)C(C)=C(CC)OC3=O)C(O1)=O	[2]
1′-hexylhelipyrone (10s)	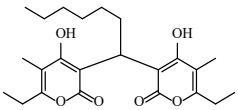	404.2199 ($C_{23}H_{32}O_6$)	dipyrones	CCC1=C(C)C(O)=C(C(CCCCCC)C2=C(O)C(C)=C(CC)OC2=O)C(O1)=O	[2]
6-diethyl-5,5,6-trimethylarzanol (11s)	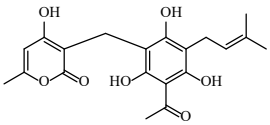	374.1365 ($C_{20}H_{22}O_7$)	3-prenyl PGs	CC1=CC(O)=C(CC2=C(O)C(C(C)=O)=C(O)C(C/C=C(C)\C)=C2O)C(O1)=O	[2]
6-diethyl-1′,5,5,6-tetramethylarzanol (12s)	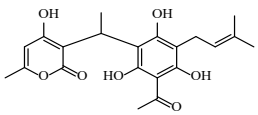	388.1522 ($C_{21}H_{24}O_7$)	3-prenyl PGs	CC1=CC(O)=C(C(C)C2=C(O)C(C(C)=O)=C(O)C(C/C=C(C)\C)=C2O)C(O1)=O	[2]
6-diethyl-5,5,6-trimethyl-1′-phenylarzanol (13s)	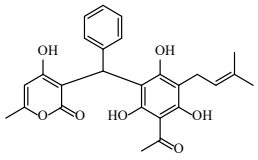	450.1678 ($C_{26}H_{26}O_7$)	3-prenyl PGs	CC1=CC(O)=C(C(C2=CC=CC=C2)C3=C(O)C(C(C)=O)=C(O)C(C/C=C(C)\C)=C3O)C(O1)=O	[2]

Table A3. *Cont.*

Compound Name	Structural Formula	Exact Mass (Da), Elem. Comp.	Class	SMILES	Reference
6-diethyl-1′-hexyl-5,5,6-trimethylarzanol (14s)	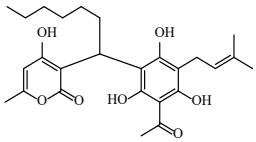	458.2304 ($C_{26}H_{34}O_7$)	3-prenyl PGs	CC1=CC(O)=C(C(CCCCCC)C2=C(O)C(C(C)=O)=C(O)C(C/C=C(C)\C)=C2O)C(O1)=O	[2]
cycloarzanol A (15s)	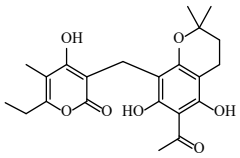	402.1678 ($C_{22}H_{26}O_7$)	3-prenyl PGs	CCC1=C(C(O)=C(C(O1)=O)CC2=C(C(C)=O)=C(C3=C2OC(C)(CC3)C)O)O)C	[1]
cycloarzanol B (16s)	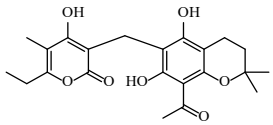	402.1678 ($C_{22}H_{26}O_7$)	3-prenyl PGs	CCC1=C(C(O)=C(C(O1)=O)CC2=C(C(C)=O)=C3OC(C)(C)CCC3=C2O)O)C	[1]
1′-methylarzanol (17s)	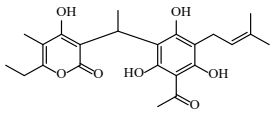	416.1835 ($C_{23}H_{28}O_7$)	3-prenyl PGs	CCC1=C(C)C(O)=C(C(C)C2=C(O)C(C(C)=O)=C(O)C(C/C=C(C)\C)=C2O)C(O1)=O	[2]
1′-phenylarzanol (18s)	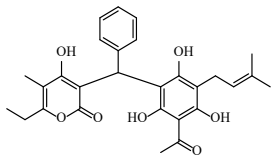	478.1991 ($C_{28}H_{30}O_7$)	3-prenyl PGs	O=C(O1)C(C(C2=CC=CC=C2)C3=C(O)C(C(C)=O)=C(O)C(C/C=C(C)\C)=C3O)=C(O)C(C)=C1CC	[2]
1′-hexylarzanol (19s)	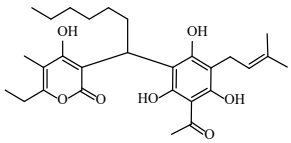	486.2617 ($C_{28}H_{38}O_7$)	3-prenyl PGs	O=C(O1)C(C(CCCCCC)C2=C(O)C(C(C)=O)=C(O)C(C/C=C(C)\C)=C2O)=C(O)C(C)=C1CC	[2]
arzanol tetra-acetate (20s)	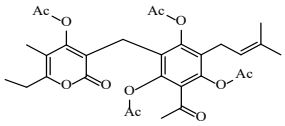	570.2101 ($C_{30}H_{34}O_{11}$)	3-prenyl PGs	CCC1=C(C)C(OC(C)=O)=C(C(O1)=O)CC2=C(C(C(C)=O)=C(C(C/C=C(C)\C)=C2OC(C)=O)OC(C)=O)OC(C)=O	[1]
6-O-desmethylaurice-pyrone tetraacetate (21s)	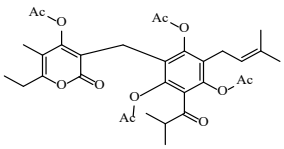	598.2414 ($C_{32}H_{38}O_{11}$)	3-prenyl PGs	O=C1C(CC2=C(C(C/C=C(C)\C)=C(C(C(C)C)=O)=C2OC(C)=O)OC(C)=O)OC(C)=O)=C(C(C)=C(O1)CC)OC(C)=O	[6]
23-methyl-6-O-desmethylaurice-pyrone tetraacetate (22s)	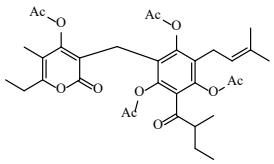	612.2571 ($C_{33}H_{40}O_{11}$)	3-prenyl PGs	O=C1C(CC2=C(C(C/C=C(C)\C)=C(C(C(CC)C)=O)=C2OC(C)=O)OC(C)=O)OC(C)=O)=C(C(C)=C(O1)CC)OC(C)=O	[6]
auricepyrone dimethyl ether (23s)	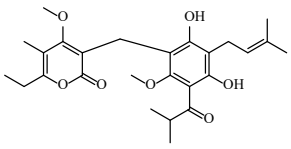	458.2304 ($C_{26}H_{34}O_7$)	3-prenyl methoxy PGs	O=C1C(CC2=C(C(C/C=C(C)\C)=C(C(C(C)C)=O)=C2OC)O)O)=C(C(C)=C(O1)CC)OC	[18]

Table A3. *Cont.*

Compound Name	Structural Formula	Exact Mass (Da), Elem. Comp.	Class	SMILES	Reference
23-methylauricepyrone dimethyl ether (24s)	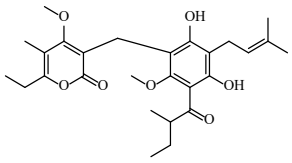	472.2461 ($C_{27}H_{36}O_7$)	3-prenyl methoxy PGs	O=C1C(CC2=C(C(C/C=C(C)\C)=C(C(C(C(CC)C)=O)=C2OC)O)O)=C(C(C)=C(O1)CC)OC	[18]
auricepyrone triacetate (25s)	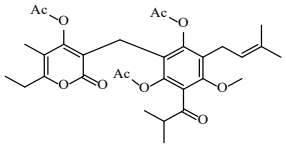	570.2465 ($C_{31}H_{38}O_{10}$)	3-prenyl methoxy PGs	O=C1C(CC2=C(C(C/C=C(C)\C)=C(C(C(C(C)C)=O)=C2OC)OC)OC)=C(C(C)=C(O1)CC)OC	[18]
23-methylauricepyrone triacetate (26s)	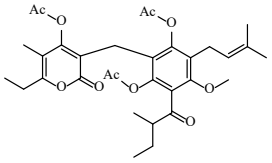	584.26215 ($C_{32}H_{40}O_{10}$)	3-prenyl methoxy PGs	O=C1C(CC2=C(C(C/C=C(C)\C)=C(C(C(C(CC)C)=O)=C2OC)OC)OC)=C(C(C)=C(O1)CC)OC	[18]
22,22-dimethylitalipyrone triacetate (27s)	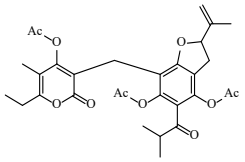	554.2152 ($C_{30}H_{34}O_{10}$)	benzopyranes	CC(C(C1)OC(C1=C2OC(C)=O)=C(C(OC(C)=O)=C2C(C(C)C)=O)CC3=C(C(C)=C(OC3=O)CC)OC(C)=O)=C	[6]
22-methyl-22-ethylitalipyrone triacetate (28s)	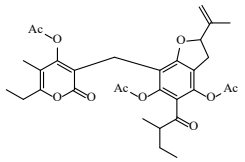	568.2308 ($C_{31}H_{36}O_{10}$)	benzopyranes	CC(C(C1)OC(C1=C2OC(C)=O)=C(C(OC(C)=O)=C2C(C(CC)C)=O)CC3=C(C(C)=C(OC3=O)CC)OC(C)=O)=C	[6]
italidipyrone tetraacetate (29s)	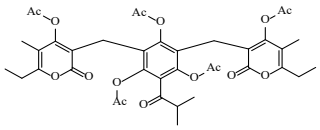	738.2524 ($C_{38}H_{42}O_{15}$)	Hetero-trimer PGs	O=C1C(CC2=C(C(CC3=C(C(C)=C(OC3=O)CC)OC(C)=O)=C(C(C(C(C)C)=O)=C2OC(C)=O)OC(C)=O)OC(C)=O)=C(C(C)=C(O1)CC)OC(C)=O	[6]
23-methylitalidipyrone tetraacetate (30s)	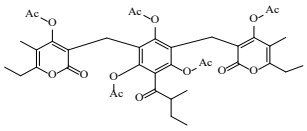	752.268 ($C_{39}H_{44}O_{15}$)	Hetero-trimer PGs	O=C1C(CC2=C(C(CC3=C(C(C)=C(OC3=O)CC)OC(C)=O)=C(C(C(C(CC)C)=O)=C2OC(C)=O)OC(C)=O)OC(C)=O)=C(C(C)=C(O1)CC)OC(C)=O	[6]

References

1. Appendino, G.; Ottino, M.; Marquez, N.; Bianchi, F.; Giana, A.; Ballero, M.; Sterner, O.; Fiebich, B.; Munoz, E. Arzanol, an anti-inflammatory and anti-HIV-1 phloroglucinol alpha-Pyrone from *Helichrysum italicum* ssp. *microphyllum*. *J. Nat. Prod.* **2007**, *70*, 608–612. [CrossRef]
2. Minassi, A.; Cicione, L.; Koeberle, A.; Bauer, J.; Laufer, S.; Werz, O.; Appendino, G. A Multicomponent Carba-Betti Strategy to Alkylidene Heterodimers–Total Synthesis and Structure–Activity Relationships of arzanol. *Eur. J. Org. Chem.* **2012**, *2012*, 772–779. [CrossRef]
3. Taglialatela-Scafati, O.; Pollastro, F.; Chianese, G.; Minassi, A.; Gibbons, S.; Arunotayanun, W.; Mabebie, B.; Ballero, M.; Appendino, G. Antimicrobial phenolics and unusual glycerides from *Helichrysum italicum* subsp. *microphyllum*. *J. Nat. Prod.* **2013**, *76*, 346–353. [CrossRef] [PubMed]

4. Ugariogu, S.; Duru, I.; Abah, C. Natural Product Chemistry and Computer Aided Drug Design an Approach to Drug Discovery: A Review Article. *Int. J. Pharmacogn. Chin. Med.* **2020**, *4*, 000207. [CrossRef]
5. Filimonov, D.; Lagunin, A.; Gloriozova, T.; Rudik, A.; Druzhilovskii, D.; Pogodin, P.; Poroikov, V. Prediction of the biological activity spectra of organic compounds using the PASS online web resource. *Chem. Heterocycl. Compd.* **2014**, *50*, 444–457. [CrossRef]
6. Hänsel, R.; Cybulski, E.-M.; Çubukçu, B.; Meriçli, A.; Bohlmann, F.; Zdero, C. Neue pyron-derivate aus Helichrysum-arten. *Phytochemistry* **1980**, *19*, 639–644. [CrossRef]
7. Akaberi, M.; Danton, O.; Tayarani-Najaran, Z.; Asili, J.; Iranshahi, M.; Emami, S.A.; Hamburger, M. HPLC-Based Activity Profiling for Antiprotozoal Compounds in the Endemic Iranian Medicinal Plant *Helichrysum oocephalum*. *J. Nat. Prod.* **2019**, *82*, 958–969. [CrossRef] [PubMed]
8. Voynikov, Y. Arzanol: A Review of Chemical Properties and Biological Activities. *Plants* **2025**, *14*, 3474. [CrossRef] [PubMed]
9. Piras, F.; Sogos, V.; Pollastro, F.; Rosa, A. Protective effect of arzanol against H_2O_2-induced oxidative stress damage in differentiated and undifferentiated SH-SY_5Y Cells. *Int. J. Mol. Sci.* **2024**, *25*, 7386. [CrossRef] [PubMed]
10. Piras, F.; Sogos, V.; Pollastro, F.; Appendino, G.; Rosa, A. Arzanol, a natural phloroglucinol α-pyrone, protects HaCaT keratinocytes against H_2O_2-induced oxidative stress, counteracting cytotoxicity, reactive oxygen species generation, apoptosis, and mitochondrial depolarization. *J. Appl. Toxicol.* **2024**, *44*, 720–732. [CrossRef] [PubMed]
11. Rosa, A.; Pollastro, F.; Atzeri, A.; Appendino, G.; Melis, M.P.; Deiana, M.; Incani, A.; Loru, D.; Dessì, M.A. Protective role of arzanol against lipid peroxidation in biological systems. *Chem. Phys. Lipids* **2011**, *164*, 24–32. [CrossRef] [PubMed]
12. Rosa, A.; Deiana, M.; Atzeri, A.; Corona, G.; Incani, A.; Melis, M.; Appendino, G.; Dessì, M. Evaluation of the antioxidant and cytotoxic activity of arzanol, a prenylated alpha-pyrone-phloroglucinol etherodimer from *Helichrysum italicum* subsp. *microphyllum*. *Chem. Biol. Interact.* **2007**, *165*, 117–126. [CrossRef] [PubMed]
13. Werner, J.; Ebrahim, W.; Özkaya, F.C.; Mándi, A.; Kurtán, T.; El-Neketi, M.; Liu, Z.; Proksch, P. Pyrone derivatives from *Helichrysum italicum*. *Fitoterapia* **2019**, *133*, 80–84. [CrossRef] [PubMed]
14. Les, F.; Venditti, A.; Cásedas, G.; Frezza, C.; Guiso, M.; Sciubba, F.; Serafini, M.; Bianco, A.; Valero, M.S.; López, V. Everlasting flower (*Helichrysum stoechas* Moench) as a potential source of bioactive molecules with antiproliferative, antioxidant, antidiabetic and neuroprotective properties. *Ind. Crops Prod.* **2017**, *108*, 295–302. [CrossRef]
15. Rosa, A.; Atzeri, A.; Nieddu, M.; Appendino, G. New insights into the antioxidant activity and cytotoxicity of arzanol and effect of methylation on its biological properties. *Chem. Phys. Lipids* **2017**, *205*, 55–64. [CrossRef] [PubMed]
16. Bauer, J.; Koeberle, A.; Dehm, F.; Pollastro, F.; Appendino, G.; Northoff, H.; Rossi, A.; Sautebin, L.; Werz, O. Arzanol, a prenylated heterodimeric phloroglucinyl pyrone, inhibits eicosanoid biosynthesis and exhibits anti-inflammatory efficacy In Vivo. *Biochem. Pharmacol.* **2011**, *81*, 259–268. [CrossRef] [PubMed]
17. Borgonetti, V.; Caroli, C.; Governa, P.; Virginia, B.; Pollastro, F.; Franchini, S.; Manetti, F.; Les, F.; López, V.; Pellati, F.; et al. *Helichrysum stoechas* (L.) Moench reduces body weight gain and modulates mood disorders via inhibition of silent information regulator 1 (SIRT1) by arzanol. *Phytother. Res.* **2023**, *37*, 4304–4320. [CrossRef] [PubMed]
18. Bohlmann, F.; Zdero, C. Neue phloroglucin-derivate aus *Helichrysum*-arten. *Phytochemistry* **1980**, *19*, 153–155. [CrossRef]
19. Opitz, L.; Hänsel, R. Helipyron, ein methylen-bis-triacetsäurelacton aus *helichrysum italicum*. *Tetrahedron Lett.* **1970**, *11*, 3369–3370. [CrossRef]
20. Bigi, F.; Casiraghi, G.; Casnati, G.; Sartori, G. Modification of the Nickl Reaction: A General Synthetic Approach to 2-Vinyl-2,3-dihydrobenzofurans. *Tetrahedron* **1983**, *39*, 169–174. [CrossRef]
21. Minassi, A.; Giana, A.; Ech-Chahad, A.; Appendino, G. Total Synthesis of arzanol, a Prenylated Heterodimeric Phloroglucinyl Pyrone from *Helichrysum italicum*. *Org. Lett.* **2008**, *10*, 2267–2270. [CrossRef] [PubMed]
22. Zhang, J.; Xiong, W.; Wen, Y.; Fu, X.; Lu, X.; Zhang, G.; Wang, C. Magnesium Dicarboxylates Promote the Prenylation of Phenolics That Is Extended to the Total Synthesis of Icaritin. *Org. Biomol. Chem.* **2022**, *20*, 1096–1100. [CrossRef] [PubMed]
23. Wei, G.; Chalker, J.M.; Cohen, T. Synthesis of (−)-α-Kainic Acid via TMSCl-Promoted Pd-Catalyzed Zinc-ene Cyclization of an Allyl Acetate. *J. Org. Chem.* **2011**, *76*, 7912–7917. [CrossRef] [PubMed]
24. Pàmies, O.; Margalef, J.; Cañellas, S.; James, J.; Judge, E.; Guiry, P.J.; Moberg, C.; Bäckvall, J.-E.; Pfaltz, A.; Pericàs, M.A.; et al. Recent Advances in Enantioselective Pd-Catalyzed Allylic Substitution: From Design to Applications. *Chem. Rev.* **2021**, *121*, 4373–4505. [CrossRef] [PubMed]
25. Yang, J.; Lao, J.; Guo, D.; Huang, W. Total Synthesis of (±)-5,3′-Dihydroxy-4′-methoxy-6″,6″-dimethyl-chromeno-(7,8,2″,3″)-flavanone. *Chin. J. Org. Chem.* **2012**, *32*, 1749–1752. [CrossRef]
26. Svouraki, A.; Garscha, U.; Kouloura, E.; Pace, S.; Pergola, C.; Krauth, V.; Rossi, A.; Sautebin, L.; Halabalaki, M.; Werz, O.; et al. Evaluation of Dual 5-Lipoxygenase/Microsomal Prostaglandin E2 Synthase-1 Inhibitory Effect of Natural and Synthetic Acronychia-Type Isoprenylated Acetophenones. *J. Nat. Prod.* **2017**, *80*, 699–706. [CrossRef] [PubMed]
27. Azam, U.; Naseer, M. Synthesis and DNA binding studies of novel sulfanilamide-linked isatin-hydrazide conjugates: Spectral and computational insights. *J. Mol. Struct.* **2025**, *1340*, 142491. [CrossRef]

28. Giercuszkiewicz-Haśnik, K.; Skonieczna, M.; Morak-Młodawska, B.; Jeleń, M. Design, Synthesis, and Testing of 1,2,3-Triazolo-Quinobenzothiazine Hybrids for Cytotoxic and Immunomodulatory Activity. *Int. J. Mol. Sci.* **2025**, *26*, 6920. [CrossRef] [PubMed]
29. Mushtaq, A.; Naseer, M. New Trisubstituted s-Triazine Derivatives: Synthesis, Characterization, DNA Binding Studies, and Computational Insights. *Chem. Sel.* **2025**, *10*, e01774. [CrossRef]
30. Mishra, G.; Tripathy, S.; Pattanayak, P. Novel Urea Substituted Benzimidazole Derivatives as Anthelmintics: In Silico and In Vitro Approaches. *Russ. J. Bioorg. Chem.* **2024**, *50*, 962–973. [CrossRef]
31. Heo, H.-S.; Cho, M.; Chung, K.-S.; Lee, C.-W.; Yoon, Y.-S.; Lee, S.-H.; An, H.-J.; Lee, K.-T. In vitro and in vivo anti-inflammatory and chondroprotective effects of standardized hot water extract from *Hydrangea serrata* (Thunb.) Ser. via modulation of NF-κB and MAPK pathways. *J. Ethnopharmacol.* **2025**, *353*, 120321. [CrossRef] [PubMed]
32. Shabayek, S.; Abdelhammed, R.; Ahmed, S. The antifungal, antibacterial, and antiviral activities of a Echinosterol isolated from the red sea Echinoclathria sponge. *Microb. Pathog.* **2025**, *206*, 107772. [CrossRef] [PubMed]
33. Jaiswal, N.; Kumar, A. Bioactive Phytophenolics of Vitex negundo Reveal Therapeutic Antifungal Potentials against Candida albicans. *Chin. J. Integr. Med.* **2025**, *31*, 541–551. [CrossRef] [PubMed]
34. Maaji, A.; Dhakar, R.; Teli, P.; Garu, U.; Adamu, U.; Muhammad, S.; Jubril, K.; Sambo, F. In-silico evaluation of Cassia occidentalis phytochemicals for Plasmodium falciparum plasmepsin V inhibition: Revealing antimalarial potential. *S. Afr. J. Bot.* **2025**, *177*, 527–541. [CrossRef]
35. Arthur, M.N.; Hanson, G.; Broni, E.; Sakyi, P.O.; Mensah-Brown, H.; Miller, W.A., III; Kwofie, S.K. Natural Product Identification and Molecular Docking Studies of Leishmania Major Pteridine Reductase Inhibitors. *Pharmaceuticals* **2025**, *18*, 6. [CrossRef] [PubMed]
36. Peng, Y.; Liu, H.; Liu, J.; Long, J. Post-translational modifications on mitochondrial metabolic enzymes in cancer. *Free Radic. Biol. Med.* **2022**, *179*, 11–23. [CrossRef] [PubMed]
37. Esser, L.; Xia, D. Mitochondrial Cytochrome bc1 Complex as Validated Drug Target: A Structural Perspective. *Trop. Med. Infect. Dis.* **2024**, *9*, 39. [CrossRef] [PubMed]
38. Duvenage, L.; Munro, A.; Gourlay, W. The potential of respiration inhibition as a new approach to combat human fungal pathogens. *Curr. Genet.* **2019**, *65*, 1347–1353. [CrossRef] [PubMed]
39. Chandel, S. Mitochondrial complex. III: An essential component of universal oxygen sensing machinery? *Respir. Physiol. Neurobiol.* **2010**, *174*, 175–181. [CrossRef] [PubMed]
40. Takahashi, I.; Ojima, N.; Ogura, K.; Seto, S. Purification and characterization of dimethylallyl pyrophosphate: Aspulvinone dimethylallyltransferase from *Aspergillus terreus*. *Biochemistry* **1978**, *17*, 2696–2702. [CrossRef] [PubMed]
41. Ammendolia, D.; Bement, W.; Brumell, J. Plasma membrane integrity: Implications for health and disease. *BMC Biol.* **2021**, *19*, 71. [CrossRef] [PubMed]
42. Pooley, H.; Abellan, F.; Karamata, D. CDP-glycerol:poly(glycerophosphate) glycerophosphotransferase, which is involved in the synthesis of the major wall teichoic acid in Bacillus subtilis 168, is encoded by tagF (rodC). *J. Bacteriol.* **1992**, *174*, 646–649. [CrossRef] [PubMed]
43. Fitzgerald, S.; Foster, T. Molecular Analysis of the tagF Gene, Encoding CDP-Glycerol:Poly(glycerophosphate) Glycerophosphotransferase of *Staphylococcus epidermidis* ATCC 14990. *J. Bacteriol.* **2000**, *182*, 1046–1052. [CrossRef] [PubMed]
44. Brown, S.; Santa Maria, J.; Walker, S. Wall teichoic acids of Gram-Positive bacteria. *Annu. Rev. Microbiol.* **2013**, *67*, 313–336. [CrossRef] [PubMed]
45. Liu, M.; Panda, S.K.; Luyten, W. Plant-Based Natural Products for the Discovery and Development of Novel Anthelmintics against Nematodes. *Biomolecules* **2020**, *10*, 426. [CrossRef] [PubMed]
46. Taylor, C.; Wang, Q.; Rosa, B.; Huang, S.; Powell, K.; Schedl, T.; Pearce, E.; Abubucker, S.; Mitreva, M. Discovery of anthelmintic drug targets and drugs using chokepoints in nematode metabolic pathways. *PLoS Pathog.* **2013**, *9*, e1003505. [CrossRef] [PubMed]
47. Partridge, F.A.; Forman, R.; Bataille, C.J.R.; Wynne, G.M.; Nick, M.; Russell, A.J.; Else, K.J.; Sattelle, D.B. Anthelmintic drug discovery: Target identification, screening methods and the role of open science. *Beilstein J. Org. Chem.* **2020**, *16*, 1203–1224. [CrossRef] [PubMed]
48. Zhang, H.; Xu, J.; Long, Y.; Maimaitijiang, A.; Su, Z.; Li, W.; Li, J. Unraveling the Guardian: P53's Multifaceted Role in the DNA Damage Response and Tumor Treatment Strategies. *Int. J. Mol. Sci.* **2024**, *25*, 12928. [CrossRef] [PubMed]
49. Ashcroft, M.; Taya, Y.; Vousden, K. Stress signals utilize multiple pathways to stabilize p53. *Mol. Cell. Biol.* **2000**, *20*, 3224–3233. [CrossRef] [PubMed]
50. Hernández Borrero, L.; El-Deiry, W. Tumor suppressor p53: Biology, signaling pathways, and therapeutic targeting. *Biochim. Biophys. Acta Rev. Cancer* **2021**, *1876*, 188556. [CrossRef] [PubMed]
51. Ohba, H.; Inano, H.; Tamaoki, B. Kinetic mechanism of porcine testicular 17 beta-hydroxysteroid dehydrogenase. *J. Steroid Biochem.* **1982**, *17*, 381–386. [CrossRef] [PubMed]
52. Poirier, D. Inhibitors of 17 beta-hydroxysteroid dehydrogenases. *Curr. Med. Chem.* **2003**, *10*, 453–477. [CrossRef] [PubMed]

53. Moeller, G.; Adamski, J. Integrated view on 17beta-hydroxysteroid dehydrogenases. *Mol. Cell. Endocrinol.* **2009**, *301*, 7–19. [CrossRef] [PubMed]
54. Hilborn, E.; Stal, O.; Jansson, A. Estrogen and androgen-converting enzymes 17β-hydroxysteroid dehydrogenase and their involvement in cancer: With a special focus on 17β-hydroxysteroid dehydrogenase type 1, 2, and breast cancer. *Oncotarget* **2017**, *8*, 30552–30562. [CrossRef] [PubMed]
55. He, W.; Gauri, M.; Li, T.; Wang, R.; Lin, S. Current knowledge of the multifunctional 17β-hydroxysteroid dehydrogenase type 1 (HSD17B1). *Gene* **2016**, *588*, 54–61. [CrossRef] [PubMed]
56. Poirier, D. Recent advances in the development of 17beta-hydroxysteroid dehydrogenase inhibitors. *Steroids* **2025**, *213*, 109529. [CrossRef] [PubMed]
57. Bezek, K.; Kramberger, K.; Barlič-Maganja, D. Antioxidant and Antimicrobial Properties of *Helichrysum italicum* (Roth) G. Don Hydrosol. *Antibiotics* **2022**, *28*, 1017. [CrossRef] [PubMed]
58. Ninčević, T.; Grdiša, M.; Šatović, Z.; Jug-Dujaković, M. *Helichrysum italicum* (Roth) G. Don: Taxonomy, biological activity, biochemical and genetic diversity. *Ind. Crops Prod.* **2019**, *138*, 111487. [CrossRef]
59. Kothavade, P.; Nagmoti, D.; Bulani, V.; Juvekar, A. Arzanol, a Potent mPGES-1 Inhibitor:Novel Anti-Inflammatory Agent. *Sci. World J.* **2013**, *2013*, 986429. [CrossRef] [PubMed]
60. Sala, A.; Recio, M.; Giner, R.; Máñez, S.; Tournier, H.; Schinella, G.; Ríos, J. Anti-inflammatory and antioxidant properties of *Helichrysum italicum*. *J. Pharm. Pharmacol.* **2002**, *54*, 365–371. [CrossRef] [PubMed]
61. Lagunin, A.; Zakharov, A.; Filimonov, D.; Poroikov, V. QSAR modelling of rat acute toxicity on the basis of PASS prediction. *Mol. Inform.* **2011**, *30*, 241–250. [CrossRef] [PubMed]
62. Salman, S.; Shah, F.; Lee, H.-W. Chromium chelated carrageenan: An investigation of physicochemical properties, toxicity, and antimicrobial potential through a computational and experimental approach. *Lett. Drug Des. Discov.* **2025**, *22*, 100006. [CrossRef]
63. Naki, T.; Matshe, W.; Obisesan, O.; Balogun, M.; Oselusi, S.; Ray, S.; Aberibigbe, B. Design, in Silico, and In Vitro Evaluation of Polymer-Based Drug Conjugates Incorporated with Derivative of Cinnamic Acid, Zidovudine, and 4-Aminosalicylic Acid against Pseudo-HIV-1. *Curr. HIV Res.* **2024**, *22*, 374–390. [CrossRef] [PubMed]
64. Raheem, K.; Ibukunoluwa, F.; Olorundare, S.; Nandwa, J.; Abayomi, M.; Uchechukwu, E.; Adewunmi, M.; Blessing, K.; Anthony, M.; Gbadebo, M.; et al. Therapeutic capability of selected medicinal plants' bioactive constituents against the mutant ovarian TP53 gene; a computational approach. *Adv. Biomark. Sci. Technol.* **2023**, *5*, 8–32. [CrossRef]
65. Beaumont, K.; Webster, R.; Gardner, I.; Dack, K. Design of ester prodrugs to enhance oral absorption of poorly permeable compounds: Challenges to the discovery scientist. *Curr. Drug Metab.* **2003**, *4*, 461–485. [CrossRef] [PubMed]
66. Dahan, A.; Zimmermann, E.; Ben-Shabat, S. Modern prodrug design for targeted oral drug delivery. *Molecules* **2014**, *19*, 16489–16505. [CrossRef] [PubMed]
67. Zhou, G. Exploring Ester Prodrugs: A Comprehensive Review of Approaches, Applications, and Methods. *Pharmacol. Pharm.* **2024**, *15*, 269–284. [CrossRef]
68. Waring, M. Lipophilicity in drug discovery. *Expert Opin. Drug Discov.* **2010**, *5*, 235–248. [CrossRef] [PubMed]
69. Arnott, J.; Planey, S. The influence of lipophilicity in drug discovery and design. *Expert Opin. Drug Discov.* **2012**, *10*, 863–875. [CrossRef] [PubMed]
70. Lipinski, C.; Lombardo, F.; Dominy, B.; Feeney, P. Experimental and computational approaches to estimate solubility and permeability in drug discovery and development settings. *Adv. Drug Deliv. Rev.* **2001**, *46*, 3–26. [CrossRef] [PubMed]
71. Adachi, K.; Shimizu, M.; Shono, F.; Funatsu, K.; Yamazaki, H. Octanol/water partition coefficient estimated using retention times in reverse-phase liquid chromatography and calculated in silico as one of the determinant factors for pharmacokinetic parameter estimations of general chemical substances. *J. Toxicol. Sci.* **2024**, *49*, 127–137. [CrossRef] [PubMed]
72. Klimoszek, D.; Dołowy, M.; Jeleń, M.; Bober-Majnusz, K. Use of TLC and Computational Methods to Determine Lipophilicity Parameters of Selected Neuroleptics: Comparison of Experimental and Theoretical Studies. *Pharmaceuticals* **2025**, *18*, 1255. [CrossRef] [PubMed]